RESEARCH ARTICLE

Cytoplasmic sharing through apical membrane remodeling

Nora G Peterson[1], Benjamin M Stormo[1], Kevin P Schoenfelder[2], Juliet S King[3], Rayson RS Lee[4], Donald T Fox[1,2,3]*

[1]Department of Cell Biology, Duke University Medical Center, Durham, United States; [2]University Program in Genetics and Genomics, Duke University, Durham, United States; [3]Department of Pharmacology & Cancer Biology, Duke University Medical Center, Durham, United States; [4]Duke-NUS Medical School, Singapore, Singapore

Abstract Multiple nuclei sharing a common cytoplasm are found in diverse tissues, organisms, and diseases. Yet, multinucleation remains a poorly understood biological property. Cytoplasm sharing invariably involves plasma membrane breaches. In contrast, we discovered cytoplasm sharing without membrane breaching in highly resorptive *Drosophila* rectal papillae. During a six-hour developmental window, 100 individual papillar cells assemble a multinucleate cytoplasm, allowing passage of proteins of at least 62 kDa throughout papillar tissue. Papillar cytoplasm sharing does not employ canonical mechanisms such as incomplete cytokinesis or muscle fusion pore regulators. Instead, sharing requires gap junction proteins (normally associated with transport of molecules < 1 kDa), which are positioned by membrane remodeling GTPases. Our work reveals a new role for apical membrane remodeling in converting a multicellular epithelium into a giant multinucleate cytoplasm.

***For correspondence:** don.fox@duke.edu

Competing interests: The authors declare that no competing interests exist.

Funding: See page 31

Received: 21 April 2020
Accepted: 13 October 2020
Published: 14 October 2020

Reviewing editor: Elaine Fuchs, Howard Hughes Medical Institute, The Rockefeller University, United States

Introduction

Throughout the tree of life, there are upper limits to the size of individual cells. This size limitation is imposed by genome content, which impacts biosynthetic capacity and cell growth (***Conlon and Raff, 1999***; ***Mueller, 2015***). In diverse tissues and organisms, the existence of 'giant cells' is driven by polyploidy, the presence of greater than a diploid genome content (***Van de Peer et al., 2017***; ***Schoenfelder and Fox, 2015***). Purposes of polyploidy across evolution remain largely unknown. However, one potential advantage of a tissue containing few, large polyploid cells vs. numerous, small diploid cells is the ability of cytoplasmic components to move over much larger distances.

A common form of polyploidy is multinucleation. Sharing of cytoplasm in a multinucleate tissue or organism is an important and recurring adaptation across evolution. Multinucleate cells can be large, metabolically-active cells with unique shapes and functions ranging from specialized force distribution to tissue barrier preservation. During organismal development, examples of multinucleation include animal skeletal muscle, mammalian osteoclasts, and mammalian syncytial placental trophoblasts (***Deng et al., 2017***; ***Gerbaud and Pidoux, 2015***; ***Pereira et al., 2018***). Multinucleation also arises in response to tissue stress, such as following injury to the *Drosophila* abdominal epithelium or the human corneal epithelium (***Losick et al., 2013***; ***Ikebe et al., 1986***). A commonality of these numerous examples of multinucleation is the ability to exchange, over long distances, cytoplasmic components such as RNA, proteins, and even organelles (***Rustom et al., 2004***; ***McLean and Cooley, 2013***).

The cellular mechanisms underlying multinucleation are diverse. During cell division, multinucleation can occur through incomplete cytokinesis, followed by formation of a stable cytoplasmic bridge between nuclei. This process occurs in diverse examples of germ cell development

eLife digest Most cells are self-contained – they have a cell membrane that delimits and therefore defines the cell, separating it from other cells and from its environment. But sometimes several cells interconnect and form collectives so they can pool their internal resources. Some of the best-known examples of this happen in animal muscle cells and in the placenta of mammals. These cell collectives share their cytoplasm – the fluid within the cell membrane that contains the cell organelles – in one of two ways. Cells can either remain linked instead of breaking away when they divide, or they can fuse their membranes with those of their neighbors. Working out how cells link to their neighbors is difficult when so few examples of cytoplasm sharing are available for study. One way to tackle this is to try and find undiscovered cell collectives in an animal that is already heavily studied in the lab, such as the fruit fly *Drosophila melanogaster*.

Peterson et al. used a genetic system that randomly labels each cell of the developing fly with one of three fluorescent proteins. These proteins are big and should not move between cells unless they are sharing their cytoplasm. This means that any cell containing two or more different colors of fluorescent protein must be connected to at least one of its neighbors. The experiment revealed that the cells of the fruit fly rectum share their cytoplasm in a way never seen before. This sharing occurs at a consistent point in the development of the fruit fly and uses a different set of genes to those used by interconnecting cells in mammal muscles and placenta. These genes produce proteins that reshape the membranes of the cells and fit them with gap junctions – tiny pores that cross from one membrane to the next, allowing the passage of very small molecules. In this case, the gap junctions allowed the cells to share molecules much larger than seen before. The result is a giant cell membrane containing the cytoplasm and organelles of more than a hundred individual cells.

These findings expand scientists' understanding of how cells in a tissue can share cytoplasm and resources. They also introduce a new tissue in the fruit fly that can be used in future studies of cytoplasm sharing. Relatives of fruit flies, including fruit pests and mosquitos, have similar cell structure to the fruit fly, which means that further investigations using this system could result in advances in agriculture or human health.

(**Greenbaum et al., 2011**) and also in some somatic cells such as the ring canal of the *Drosophila* ovary (**McLean and Cooley, 2013**) and the plasmodesmata of plants (**Lůcas and Wolf, 1993**). A second major mechanism of multinucleation involves plasma membrane breaches. Such breaches can involve distinct actin-based protrusive structures. Podosome-like structures facilitate multinucleation in *Drosophila* skeletal muscle and mammalian macrophages (**Faust et al., 2019**; **Sens et al., 2010**). While the mechanisms are diverse, one common feature of the above-discussed examples of multinucleation and cytoplasm sharing identified to date are clearly visible plasma membrane disruptions.

Here, we report a visual animal-wide screen, using multi-color lineage labeling approaches in the tractable animal model *Drosophila melanogaster,* for multinucleate tissues that share cytoplasm. We discover cytoplasm sharing in the rectal papilla, a common insect resorptive intestinal epithelium that is critical for maintaining ionic homeostasis (**Wigglesworth, 1932**; **Cohen et al., 2020**). Likely due to its extreme proximal location in the gut of many insect species, this epithelium is linked to the infiltration of diverse pathogens, such as those involved in African sleeping sickness and also viruses being pursued as insect control measures (**Gu et al., 2010**; **Filosa et al., 2019**). Here, we reveal that cytoplasm sharing onset in *Drosophila* papillae occurs during a short developmental window, indicating robust molecular regulation. We find that papillar cytoplasm sharing requires neither incomplete cytokinesis nor canonical actin-based membrane breach regulators. Using transmission electron microscopy, we further identify that this developmentally programmed process involves extensive remodeling of apical junctions and lateral membranes, but not clearly identifiable plasma membrane breaches. Using genetic screening, we implicate specific regulators of membrane remodeling, notably the GTPase Dynamin/Shibire, in the mechanism of papillar cytoplasmic sharing. From analysis of *shibire* mutants, we uncover a requirement for gap junction establishment and specific gap junction proteins in papillar cytoplasm sharing. Mutant animals defective in papillar cytoplasm sharing are intolerant of a high-salt diet, indicating a physiological role of long-range cytoplasm movement in this tissue. Unlike all known examples of multinucleation, our results show that

cytoplasm sharing in rectal papillae requires developmentally programmed apical membrane remodeling, which creates a giant resorptive epithelial network of 100 nuclei. This tissue represents a new system to investigate the diversity of multicellular tissue organization and mechanisms and functions of cytoplasm sharing.

Results

Drosophila hindgut papillae undergo developmentally programmed cytoplasmic sharing

To identify new examples of adult tissues in *Drosophila* that share cytoplasm, we ubiquitously expressed *Cre* and *UAS-dBrainbow* (**Hampel et al., 2011**; **Figure 1A**), a Cre-Lox-based system that randomly labels cells with only one of three fluorescent proteins. We used animals heterozygous for *UAS-dBrainbow* to ensure single-labeling of cells. We ubiquitously expressed *Cre,* which does not require heat-shock induction, from early embryonic stages (before cells endocycle to become polyploid). Cre-mediated excision occurs independently of Gal4 expression and Gal80^{ts} repression of dBrainbow. Therefore, we can ensure that multi-labeled cells only arise by cytoplasm sharing between cells not related by cell division or incomplete cytokinesis (**Figure 1B**). We examined a wide range of tissues (**Figure 1—figure supplement 1A**). From our screen, we discovered that the rectal papilla is a new example of a tissue with cytoplasm sharing. Adult *Drosophila* contain four papillae, each with 100 nuclei of genome content between 8 and 16C (**Fox et al., 2010**), that reside in the posterior hindgut (**Figure 1C**). Each papilla is a polarized epithelial cone with the apical region facing the gut lumen and the basal region surrounding a central canal that connects to the fly's hemolymph (**Figure 1D**). The papillar structure supports its function to reabsorb water, ions, and small molecules from the gut lumen and recycle them back to the hemolymph (**Cohen et al., 2020**). Knowing that adult papillar cells share cytoplasm, we next used our dBrainbow system to identify when papillar cells begin to share relative to other developmental events that we previously identified (**Figure 1E**). Using both fixed and live imaging of whole organs, we found that at 62 hours post-puparium formation (HPPF), each papillar cell contains only one dBrainbow label (**Figure 1F**). By contrast, at 69HPPF, multi-labeled cells are apparent (**Figure 1F',H–H'**). We quantitatively measured papillar sharing across the tissue (**Figure 1—figure supplement 1B**, Materials and methods) and found that cytoplasm sharing initiates over a narrow 6 hr period (68-74HPPF, **Figure 1G**). Our results suggested that at least RNA and possibly protein passes between papillar cells to facilitate cytoplasm sharing. To directly test if protein is shared, we photo-activated GFP (GFP^{PA}) in single adult papillar cells and observed in real time whether GFP^{PA} spreads to adjacent cells. We find the principal papillar cells, but not the secondary cells at the papillar base (**Garayoa et al., 1999**; **Figure 1—figure supplement 1C**), share protein across an area of at least several nuclei (**Figure 1I–I'**). We next tested whether a larger protein can be shared between papillar cells. We used rectal papillae RNA-sequencing data (**Leader et al., 2018**) to identify proteins that are endogenously expressed, cytoplasmic, and relatively large. We therefore generated flies expressing a UAS-inducible, photoactivatable GFP fused to *Glyceraldehyde 3 phosphate dehydrogenase 2* (*UAS-Gapdh2-GFP^{PA}*). This construct should produce a tagged protein of 62.3 kDa. We found that Gapdh2-GFP^{PA} protein is shared between cells, as it never stops at a papillar cell–cell boundary, though it may move at a slower rate than GFP^{PA} (**Figure 1—figure supplement 1D**). Therefore, proteins as large as ~62 kDa (the size of GFP-tagged Gapdh2) can move across an area covered by multiple papillar nuclei. Additionally, the movement of our Gapdh2 transgenic protein indicates that papillar cells likely share endogenously expressed proteins. These results indicate that papillae undergo a developmentally programmed conversion from 100 individual cells to a single giant multinuclear cytoplasm that shares the products of ~1200 genomes.

We next examined whether cytoplasm sharing requires either programmed endocycles or mitoses. We have previously shown that larval papillar cells first undergo endocycles, which increase cellular ploidy. Then, during metamorphosis, pupal papillar cells disassemble polytene chromosomes and undergo polyploid mitotic cycles, which increase cell number (**Fox et al., 2010**; **Stormo and Fox, 2016**; **Stormo and Fox, 2019**). Both endocycles and mitoses occur well prior to the start of papillar cytoplasm sharing (**Figure 1E**). Papillar endocycles require the Anaphase-Promoting Complex/Cyclosome regulator *fizzy-related* (*fzr*) while the papillar mitoses require Notch signaling

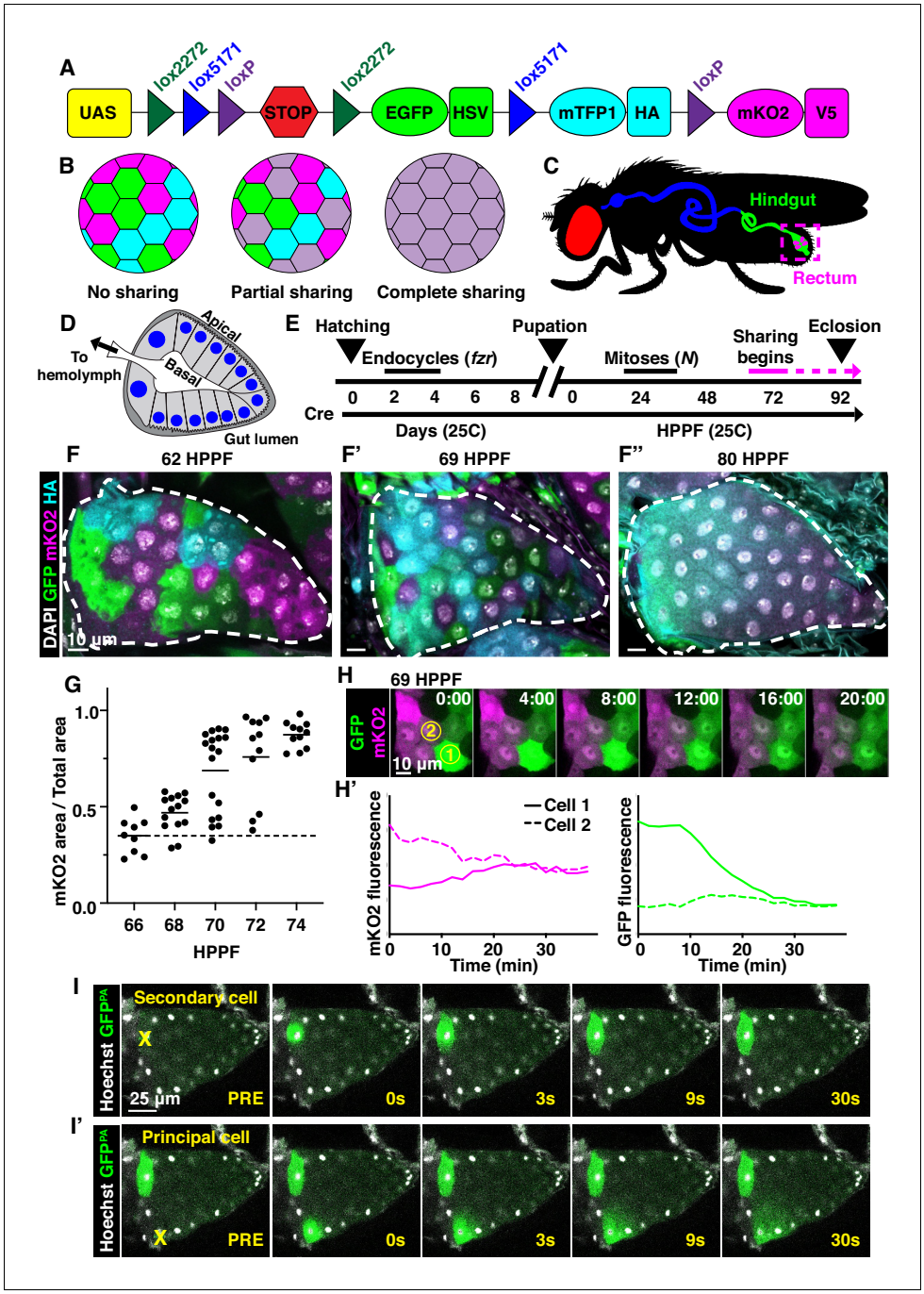

Figure 1. Developmentally programmed cytoplasmic sharing in *Drosophila* papillae. (**A**) The dBrainbow construct (***Hampel et al., 2011***). Cre recombinase randomly excises one pair of lox sites, and approximately 1/3 of cells express either EGFP, mKO2, or mTFP1. (**B**) Model of dBrainbow expression with no, partial, or complete cytoplasmic sharing. (**C**) *Drosophila* digestive tract with rectum containing four papillae labeled in magenta box. (**D**) Cartoon of a cross-section through an adult rectal papilla. The papilla consists of an epithelial cone with the apical region facing the gut lumen and the interior basal region facing a central canal leading to the fly hemolymph. The principal papillar cells have microvilli-like projections on the apical edge. One layer of larger, secondary cells forms the base of the papilla. The papilla is covered in a cuticle layer (dark gray). Nuclei are marked in blue. (**E**) Approximate timeline of ubiquitous Cre induction and cytoplasm sharing onset (68–74 HPPF) within papillar development (***Fox et al., 2010***). Cytoplasmic sharing is temporally separate from papillar mitoses. (**F–F''**) Representative *dBrainbow* papillae at 62 (**F**), 69 (**F'**), or 80 (**F''**) hours post-puparium formation (HPPF). (**G**) Cytoplasmic sharing quantification during pupal development. Lines = mean at each time, which differs

Figure 1 continued on next page

Figure 1 continued

significantly between 66 and 74 HPPF ($p<0.0001$). Each point = 1 animal (N = 9–18, rep = 2). (**H**) Live *dBrainbow*-labeled papillar cells during cytoplasmic sharing (69 HPPF). (**H'**) Fluorescence of neighboring cells in (**H**). (**I–I'**) Representative adult papilla expressing photo-activatable GFP (GFP^{PA}). Single cells were photo-activated (yellow X) in secondary cells (**I**) and principal cells (**I'**). Time = seconds after activation.

The online version of this article includes the following figure supplement(s) for figure 1:

Figure supplement 1. The hindgut rectal papillae share cytoplasm independent of mitosis.

(***Schoenfelder et al., 2014***). Knockdown of *fzr* significantly disrupts cytoplasm sharing (***Figure 1—figure supplement 1E,F,H***). We hypothesize that endocycles are required for differentiation of the papillae, which later enables these cells to trigger cytoplasm sharing. In contrast, blocking Notch signaling, which initiates papillar mitotic divisions (***Fox et al., 2010***), does not prevent sharing (***Figure 1—figure supplement 1E,G,H***). Thus, papillar cytoplasm sharing requires developmentally programmed endocycles but not mitotic cycles.

Cytoplasmic sharing requires membrane remodeling proteins

As our *dBrainbow* approach only identifies cytoplasm sharing events that do not involve incomplete division/cytokinesis, we examined whether sharing results from fusion pore formation, as in skeletal muscle. A well-studied model of such cell–cell fusion in *Drosophila* is myoblast fusion, which requires an actin-based podosome (***Richardson et al., 2007***; ***Sens et al., 2010***). We conducted a candidate *dBrainbow*-based RNAi screen (77 genes, ***Figure 2A***, ***Table 1***) of myoblast fusion regulators and other plasma membrane components. Remarkably, 0/15 myoblast fusion genes from our initial screen regulate papillar cytoplasm sharing (***Figure 2A***, ***Figure 2—figure supplement 1A***, ***Table 1***). Furthermore, dominant-negative forms of Rho family GTPases have no impact on *dBrainbow* labeling (***Figure 2—figure supplement 1B***), providing additional evidence against actin-based cytoplasm sharing. Instead, we found 8/77 genes, including subunits of the vacuolar H+ ATPase (*Vha16-1*), ESCRT-III complex (*Vps2*), and exocyst (*Exo84*) (***Figure 2A***) are required for papillar cytoplasm sharing. Through additional screening, the only myoblast fusion regulator required for papillar cytoplasm sharing is *singles bar* (*sing*), a presumed vesicle trafficking gene (***Estrada et al., 2007***; ***Figure 2—figure supplement 1A***). Given the enrichment of our candidate screen hits in membrane trafficking and not myoblast fusion, we further explored the role of membrane trafficking in cytoplasm sharing.

We conducted two secondary *dBrainbow* screens to find specific membrane trafficking pathway components that regulate papillar sharing. First, a focused candidate membrane trafficking screen revealed additional components (12/36 genes screened, ***Figure 2B***, ***Table 2***) including three more vacuolar H+ ATPase subunits, five more exocyst components, and the Dynamin GTPase *shibire* (*shi*) (***Figure 2B,D,E,H***). Second, we screened constitutively-active and dominant-negative versions of all 31 *Drosophila* Rabs. Sharing requires only a small number of Rabs, specifically the ER/Golgi-associated *Rab1,* the early endosome-associated *Rab5,* and the recycling endosome-associated *Rab11* (***Figure 2C,D,F–H***). Given our identification of the membrane vesicle recycling circuit involving *shi*, *Rab5*, and *Rab11*, we focused on these genes. Two unique RNAi lines for each gene show consistent sharing defects, and most of these knockdowns completely recapitulate the pre-sharing state (***Figure 2H***). Despite exhibiting strong cytoplasm sharing defects, *shi*, *Rab5*, and *Rab11 RNAi* papillae appear morphologically normal, with only minor cell number decreases (***Figure 2—figure supplement 1C***). These results suggest that membrane recycling GTPases regulate a specific developmental event associated with cytoplasm sharing, and not papillar morphogenesis. In agreement with these GTPases acting during development, rather than as part of an ongoing transport process, GTPase knockdown after sharing onset does not block cytoplasm sharing (***Figure 2—figure supplement 1D–F***). Together, our screens reveal that membrane trafficking, particularly Dynamin-mediated endocytosis and early/recycling endosome trafficking, regulates papillar cytoplasmic sharing.

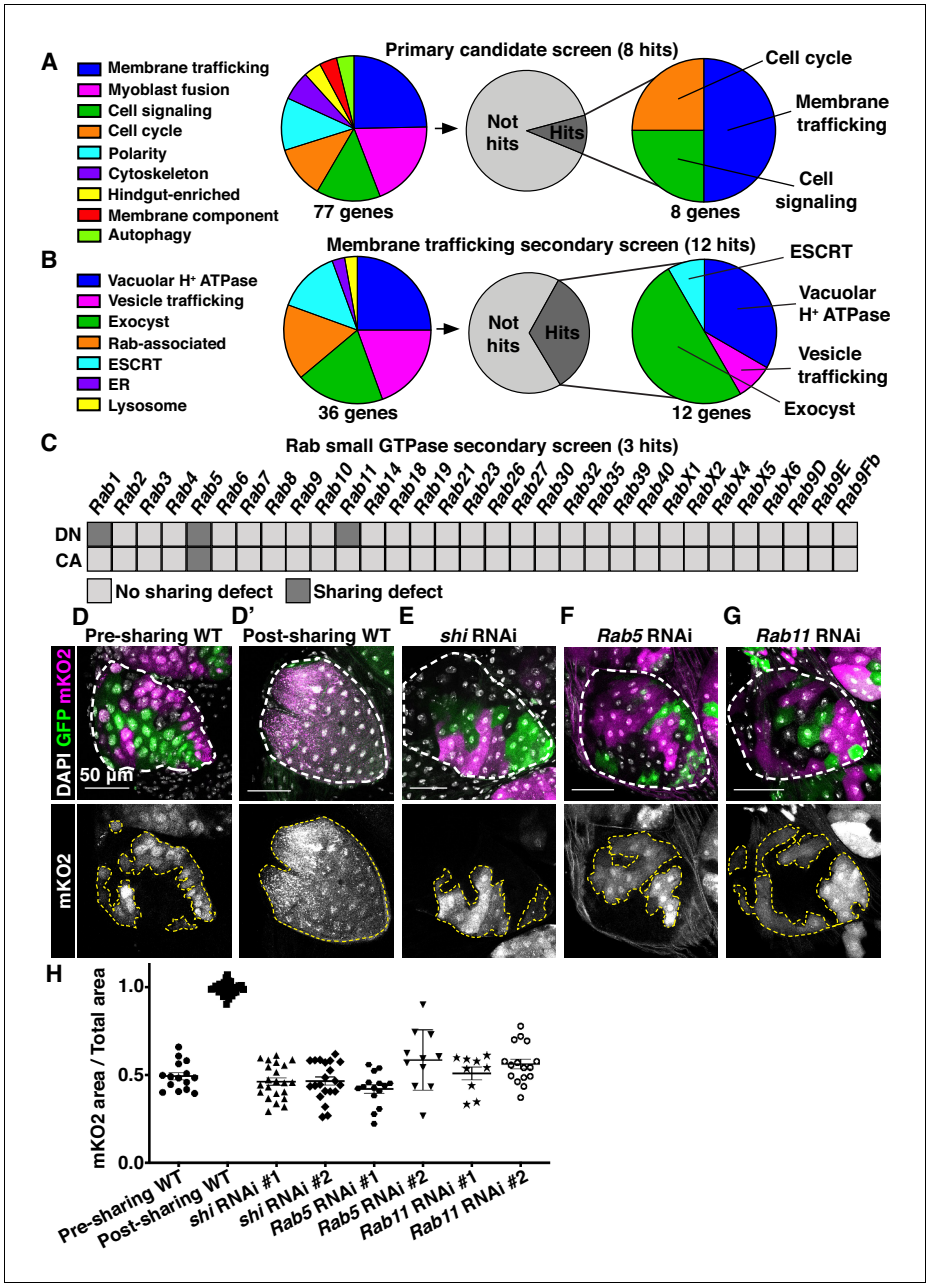

Figure 2. Cytoplasmic sharing requires membrane remodeling proteins. (**A**) Primary *dBrainbow* candidate screen. RNAi and dominant-negative versions of 77 genes representing the indicated roles were screened for sharing defects, and eight genes were identified. (**B**) Secondary membrane trafficking screen. 36 genes were screened with 12 sharing genes identified. (**C**) Secondary screen of dominant-negative and constitutively-active Rab GTPases. (**D–G**) Representative *dBrainbow* in (**D–D'**) wild type (WT) (**D**) pre-sharing (48HPPF) and (**D'**) post-sharing (young adults), (**E**) adult *shi RNAi*, (**F**) adult *Rab5 RNAi*, (**G**) adult *Rab11 RNAi*. (**H**) Quantification of (**D–G**), including two RNAi lines for *shi*, *Rab5*, and *Rab11*. Pre-sharing and knock downs differ significantly from post-sharing WT ($p<0.0001$, N = 9–32, rep = 2–3).

The online version of this article includes the following figure supplement(s) for figure 2:

Figure supplement 1. Membrane trafficking genes expressed during a developmental window regulate cytoplasm sharing.

Table 1. Cytoplasm sharing primary candidate screen gene results.

Gene category	Gene	Annotation symbol	Gene ID	Sharing disrupted?
Autophagy	*Atg1*	CG10967	FBgn0260945	No
Autophagy	*Atg7*	CG5489	FBgn0034366	No
Autophagy	*Atg8a*	CG32672	FBgn0052672	No
Cell cycle/Chromosomes	*blue*	NA	FBgn0283709	No
Cell cycle/Chromosomes	*CapD2*	CG1911	FBgn0039680	No
Cell cycle/Chromosomes	*Cdc2*	CG5363	FBgn0004106	Yes
Cell cycle/Chromosomes	*Clamp*	CG1832	FBgn0032979	No
Cell cycle/Chromosomes	*endos*	CG6513	FBgn0061515	No
Cell cycle/Chromosomes	*fzr*	CG3000	FBgn0262699	Yes
Cell cycle/Chromosomes	*Mi-2*	CG8103	FBgn0262519	No
Cell cycle/Chromosomes	*Rbp9*	CG3151	FBgn0010263	No
Cell cycle/Chromosomes	*SA-2*	CG13916	FBgn0043865	No
Cell signaling	*Chico*	CG5686	FBgn0024248	No
Cell signaling	*Egfr*	CG10079	FBgn0003731	Yes
Cell signaling	*grk*	CG17610	FBgn0001137	No
Cell signaling	*N*	CG3936	FBgn0004647	No
Cell signaling	*Ptp61F*	CG9181	FBgn0267487	No
Cell signaling	*rho*	CG1004	FBgn0004635	Yes
Cell signaling	*ru*	CG1214	FBgn0003295	No
Cell signaling	*spi*	CG10334	FBgn0005672	No
Cell signaling	*stet*	CG33166	FBgn0020248	No
Cell signaling	*wts*	CG12072	FBgn0011739	No
Cell signaling	*βggt-II*	CG18627	FBgn0028970	No
Cytoskeleton	*ALiX*	CG12876	FBgn0086346	No
Cytoskeleton	*Cdc42*	CG12530	FBgn0010341	No
Cytoskeleton	*DCTN1-p150*	CG9206	FBgn0001108	No
Cytoskeleton	*pav*	CG1258	FBgn0011692	No
Cytoskeleton	*wash*	CG13176	FBgn0033692	No
Hindgut-enriched	*dac*	CG4952	FBgn0005677	No
Hindgut-enriched	*Dr*	CG1897	FBgn0000492	No
Hindgut-enriched	*nrv3*	CG8663	FBgn0032946	No
Membrane component	*Flo1*	CG8200	FBgn0024754	No
Membrane component	*Flo2*	CG32593	FBgn0264078	No
Membrane component	*Iris*	CG4715	FBgn0031305	No
Myoblast fusion	*Arf51F*	CG8156	FBgn0013750	No
Myoblast fusion	*Arp2*	CG9901	FBgn0011742	No
Myoblast fusion	*Arp3*	CG7558	FBgn0262716	No
Myoblast fusion	*Ced-12*	CG5336	FBgn0032409	No
Myoblast fusion	*dock*	CG3727	FBgn0010583	No
Myoblast fusion	*hbs*	CG7449	FBgn0029082	No
Myoblast fusion	*Hem*	CG5837	FBgn0011771	No
Myoblast fusion	*mbc*	CG10379	FBgn0015513	No
Myoblast fusion	*Rac1*	CG2248	FBgn0010333	No
Myoblast fusion	*Rho1*	CG8416	FBgn0014020	No

Table 1 continued on next page

Table 1 continued

Gene category	Gene	Annotation symbol	Gene ID	Sharing disrupted?
Myoblast fusion	*rols*	CG32096	FBgn0041096	No
Myoblast fusion	*rst*	CG4125	FBgn0003285	No
Myoblast fusion	*SCAR*	CG4636	FBgn0041781	No
Myoblast fusion	*siz*	CG32434	FBgn0026179	No
Myoblast fusion	*WASp*	CG1520	FBgn0024273	No
Polarity	*Abi*	CG9749	FBgn0020510	No
Polarity	*CadN*	CG7100	FBgn0015609	No
Polarity	*cindr*	CG31012	FBgn0027598	No
Polarity	*cno*	CG42312	FBgn0259212	No
Polarity	*Gli*	CG3903	FBgn0001987	No
Polarity	*l(2)gl*	CG2671	FBgn0002121	No
Polarity	*Nrg*	CG1634	FBgn0264975	No
Polarity	*sdt*	CG32717	FBgn0261873	No
Polarity	*shg*	CG3722	FBgn0003391	No
Vesicle trafficking	*Atl*	CG6668	FBgn0039213	No
Vesicle trafficking	*Bet1*	CG14084	FBgn0260857	No
Vesicle trafficking	*Chmp1*	CG4108	FBgn0036805	No
Vesicle trafficking	*CHMP2B*	CG4618	FBgn0035589	No
Vesicle trafficking	*dnd*	CG6560	FBgn0038916	No
Vesicle trafficking	*Exo84*	CG6095	FBgn0266668	Yes
Vesicle trafficking	*lerp*	CG31072	FBgn0051072	No
Vesicle trafficking	*Rab11*	CG5771	FBgn0015790	Yes
Vesicle trafficking	*Rab23*	CG2108	FBgn0037364	No
Vesicle trafficking	*Rab4*	CG4921	FBgn0016701	No
Vesicle trafficking	*Rab7*	CG5915	FBgn0015795	No
Vesicle trafficking	*Rab8*	CG8287	FBgn0262518	No
Vesicle trafficking	*RabX4*	CG31118	FBgn0051118	No
Vesicle trafficking	*Vha16-1*	CG3161	FBgn0262736	Yes
Vesicle trafficking	*Vha55*	CG17369	FBgn0005671	No
Vesicle trafficking	*VhaAC39-1*	CG2934	FBgn0285910	No
Vesicle trafficking	*VhaAC39-2*	CG4624	FBgn0039058	No
Vesicle trafficking	*Vps2*	CG14542	FBgn0039402	Yes
Vesicle trafficking	*Vps33b*	CG5127	FBgn0039335	No
Total screen results				
Sharing disrupted	8			
No sharing phenotype	69			
Total	77			
Screen results by category				
Polarity	9			
Vesicle trafficking	19			
Myoblast fusion	15			
Cell cycle/Chromosomes	9			
Cell signaling	11			
Autophagy	3			

Table 1 continued on next page

Table 1 continued

Gene category	Gene	Annotation symbol	Gene ID	Sharing disrupted?
Cytoskeleton	5			
Hindgut-enriched	3			
Membrane component	3			
Total	77			

Gap junction establishment, but no membrane breaches, accompany cytoplasm sharing

To better understand how membrane trafficking GTPases initiate cytoplasm sharing during development, we examined endosome and Shi localization during sharing onset. We imaged a GFP-tagged pan-endosome marker (*myc-2x-FYVE*), overexpression of which should not alter endosome shape or localization (***Gillooly et al., 2000***; ***Wucherpfennig et al., 2003***), and a Venus-tagged *shi* before and after sharing. Endosomes are evenly distributed shortly before sharing, but become highly polarized at the basal membrane around the time of sharing onset (***Figure 3A–A',C***, ***Figure 3—figure supplement 1A***). This basal endosome repositioning requires Shi (***Figure 3B–C***, ***Figure 3—figure supplement 1A***) and the change in endosome localization is attributed to Rab5-positive early endosomes (***Figure 3—figure supplement 1B–B''***). Additionally, Shi localization changes from apical polarization to a uniform distribution during sharing onset (***Figure 3D–E***). These localization changes indicate that membrane trafficking factors which regulate cytoplasm sharing are highly dynamic during cytoplasm sharing onset.

To determine what membrane remodeling events underlie GTPase-dependent cytoplasm sharing, we turned to ultrastructural analysis. Adult ultrastructure and physiology of papillar cells has been examined previously in *Drosophila* (***Wessing and Eichelberg, 1973***) and related insects (***Gupta and Berridge, 1966***). These cells contain elaborate membrane networks that facilitate selective ion resorption from the gut lumen, facing the apical side of papillar cells, to the hemolymph, facing the basal side. Still, little is known about developmental processes or mechanisms governing the unique papillar cell architecture. We looked for changes in cell–cell junctions and lateral membranes that coincide with cytoplasm sharing, especially to determine if there is a physical membrane breach between cells. We identified several dramatic changes in membrane architecture. First, apical microvilli-like structures form during sharing onset (***Figure 3F–F''***). Just basal to the microvilli, apical cell–cell junctions are straight in early pupal development and compress into a more curving, tortuous morphology around the time of cytoplasm sharing onset (***Figure 3—figure supplement 1C–C''***). One of the most striking changes, coincident with Shi re-localization, is formation of pan-cellular endomembrane stacks surrounding mitochondria. These stacks are likely sites for active ion transport, such as that mediated by the P-type Na^+/K^+-ATPase, coupled to mitochondria for ATP (***Figure 3G–G''***; ***Berridge and Gupta, 1967***; ***Patrick et al., 2006***). Thus, massive apical and intracellular plasma membrane reorganization coincides with both cytoplasm sharing and Shi/endosome re-localization. We next assessed whether the extensive membrane remodeling requires Shi, Rab5, and Rab11. In *shi* and *Rab5 RNAi* animals, microvilli protrude downward, instead of upward (***Figure 3H–J***). Additionally, apical junctions do not compress as in controls (***Figure 3—figure supplement 1D–F***). Notably, membrane stacks are greatly reduced (***Figure 3K–M***). *shi RNAi* animals exhibit numerous trapped vesicles, consistent with a known role for Dynamin in membrane vesicle severing (***Damke et al., 1994***; ***Hinshaw and Schmid, 1995***; ***Figure 3L***, inset). Together, we find that Shi and endosomes extensively remodel membranes during papillar cytoplasm sharing.

Gap junction proteins are required for cytoplasmic sharing

Our extensive ultrastructural analysis did not reveal any clear breaches in the plasma membrane, despite numerous membrane alterations. Adult papillae exhibit large extracellular spaces between nuclei that eliminate the possibility of cytoplasm sharing throughout much of the lateral membrane (***Figure 3—figure supplement 2A***; ***Wessing and Eichelberg, 1973***; ***Gupta and Berridge, 1966***). Instead, through our GTPase knockdown studies, we identified a striking alteration in the apical cell–cell interface that strongly correlates with cytoplasm sharing. Specifically, *shi* animals frequently lack

Table 2. Membrane trafficking primary and secondary candidate screen gene results.

Gene category	Gene subcategory	Gene	Annotation symbol	Gene ID	Sharing disrupted?	Screen
Membrane trafficking	ER	*Atl*	CG6668	FBgn0039213	No	Primary
Membrane trafficking	ESCRT	*Chmp1*	CG4108	FBgn0036805	No	Primary
Membrane trafficking	ESCRT	*CHMP2B*	CG4618	FBgn0035589	No	Primary
Membrane trafficking	ESCRT	*lsn*	CG6637	FBgn0260940	No	Secondary
Membrane trafficking	ESCRT	*Vps2*	CG14542	FBgn0039402	**Yes**	Primary
Membrane trafficking	ESCRT	*Vps4*	CG6842	FBgn0283469	No	Secondary
Membrane trafficking	Exocyst	*Exo70*	CG7127	FBgn0266667	No	Secondary
Membrane trafficking	Exocyst	*Exo84*	CG6095	FBgn0266668	**Yes**	Primary
Membrane trafficking	Exocyst	*Sec10*	CG6159	FBgn0266673	**Yes**	Secondary
Membrane trafficking	Exocyst	*Sec15*	CG7034	FBgn0266674	**Yes**	Secondary
Membrane trafficking	Exocyst	*Sec5*	CG8843	FBgn0266670	**Yes**	Secondary
Membrane trafficking	Exocyst	*Sec6*	CG5341	FBgn0266671	**Yes**	Secondary
Membrane trafficking	Exocyst	*Sec8*	CG2095	FBgn0266672	**Yes**	Secondary
Membrane trafficking	Lysosome	*lerp*	CG31072	FBgn0051072	No	Primary
Membrane trafficking	Rab-associated	*CG41099*	CG41099	FBgn0039955	No	Secondary
Membrane trafficking	Rab-associated	*mtm*	CG9115	FBgn0025742	No	Secondary
Membrane trafficking	Rab-associated	*nuf*	CG33991	FBgn0013718	No	Secondary
Membrane trafficking	Rab-associated	*Rala*	CG2849	FBgn0015286	No	Secondary
Membrane trafficking	Rab-associated	*Rep*	CG8432	FBgn0026378	No	Secondary
Membrane trafficking	Rab-associated	*Rip11*	CG6606	FBgn0027335	No	Secondary
Membrane trafficking	Vacuolar H+ ATPase	*Vha16-1*	CG3161	FBgn0262736	**Yes**	Primary
Membrane trafficking	Vacuolar H+ ATPase	*Vha16-2*	CG32089	FBgn0028668	No	Secondary
Membrane trafficking	Vacuolar H+ ATPase	*Vha16-3*	CG32090	FBgn0028667	No	Secondary
Membrane trafficking	Vacuolar H+ ATPase	*Vha16-5*	CG6737	FBgn0032294	**Yes**	Secondary
Membrane trafficking	Vacuolar H+ ATPase	*Vha55*	CG17369	FBgn0005671	No	Primary
Membrane trafficking	Vacuolar H+ ATPase	*VhaAC39-1*	CG2934	FBgn0285910	No	Primary
Membrane trafficking	Vacuolar H+ ATPase	*VhaAC39-2*	CG4624	FBgn0039058	No	Primary
Membrane trafficking	Vacuolar H+ ATPase	*VhaPPA1-1*	CG7007	FBgn0028662	**Yes**	Secondary
Membrane trafficking	Vacuolar H+ ATPase	*VhaPPA1-2*	CG7026	FBgn0262514	**Yes**	Secondary
Membrane trafficking	Vesicle trafficking	*Bet1*	CG14084	FBgn0260857	No	Primary
Membrane trafficking	Vesicle trafficking	*Chc*	CG9012	FBgn0000319	No	Secondary
Membrane trafficking	Vesicle trafficking	*dnd*	CG6560	FBgn0038916	No	Primary
Membrane trafficking	Vesicle trafficking	*shi*	CG18102	FBgn0003392	**Yes**	Secondary
Membrane trafficking	Vesicle trafficking	*Vps29*	CG4764	FBgn0031310	No	Secondary
Membrane trafficking	Vesicle trafficking	*Vps33b*	CG5127	FBgn0039335	No	Primary
Membrane trafficking	Vesicle trafficking	*Vps35*	CG5625	FBgn0034708	No	Secondary
Total screen results						
Sharing disrupted	12					
No sharing phenotype	24					
Total	36					
Screen results by category	**Total**	**Hits**				
ER	1	0				
ESCRT	5	1				
Exocyst	7	6				

Table 2 continued on next page

Table 2 continued

Gene category	Gene subcategory	Gene	Annotation symbol	Gene ID	Sharing disrupted?	Screen
Lysosome	1	0				
Rab-associated	6	0				
Vacuolar H+ ATPase	9	4				
Vesicle trafficking	7	1				
Total	36					

apical gap junctions (***Figure 3N–O***) (p<0.0001) (***Figure 3P***, ***Figure 3—figure supplement 1H–H''***). Upon closer examination of control animal development, we find that apical gap junction-like structures arise at cytoplasm sharing onset. There is almost no gap junction-like structure before cytoplasm sharing (***Figure 4A–B***, ***Figure 2—figure supplement 1A–A''***). Given our electron micrograph results, we determined which innexins, the protein family associated with gap junctions in invertebrates (***Bauer et al., 2005***; ***Phelan et al., 1998***), are expressed in rectal papillae. From RNA-seq data (*Methods*), we determined that *ogre* (*Inx1*), *Inx2*, and *Inx3* are most highly expressed (***Figure 4C***). This combination of innexins is not unique to rectal papillae; the non-sharing brain and optic lobe (***Figure 4—figure supplement 1A***) also express high levels of all three (***Leader et al., 2018***). We examined localization of Inx3 (a gap junction component) (***Curtin et al., 1999***; ***Richard et al., 2017***), and compared it to a septate junction component, NeurexinIV (NrxIV) (***Laprise et al., 2009***). NrxIV localizes similarly both pre and post-sharing onset (***Figure 4D–D'***), indicative of persistent septate junctions remaining between papillar cells. In contrast, Inx3 organizes apically only after cytoplasm sharing (***Figure 4E–E'***, ***Figure 4—figure supplement 1B–B'***). Inx3 also does not localize to cell–cell boundaries in *shi* RNAi animals (***Figure 4C–C'***). We tested whether innexins are required for cytoplasm sharing. Knocking down these three genes individually causes mild yet significant cytoplasm sharing defects (***Figure 4F***). However, we see larger defects in animals expressing dominant-negative $ogre^{DN}$ (***Figure 4F–G***; ***Spéder and Brand, 2014***), which contains a N-terminal GFP tag that interferes with channel passage. Also, heterozygous animals containing a ten gene-deficiency spanning *ogre*, *Inx2*, and *Inx7* have more severe defects (***Figure 4F***, *Df(1) BSC867*). Finally, we tested whether cytoplasm sharing is essential for normal rectal papillar function. Rectal papillae selectively absorb water and ions from the gut lumen for transport back into the hemolymph, and excrete unwanted lumen contents (***Cohen et al., 2020***). One test of papillar function is viability following the challenge of a high-salt diet (***Bretscher and Fox, 2016***; ***Schoenfelder et al., 2014***). However, with our pan-hindgut driver *byn*-Gal4 used for all previous experiments, we noted animal lethality with *shi*, *Rab5*, and *Rab11* knockdown within a few days on control food. We observed melanization and necrosis throughout the hindgut (data not shown) which prevented us from attributing any phenotypes directly to papillar cytoplasm sharing. We therefore identified an alternative driver (*60H12*-Gal4) with rectum-specific expression during pupation and adulthood (***Figure 4—figure supplement 1D–D'***). We used this driver to express shi^{DN}. These animals display similar sharing defects as we find with *byn*-Gal4 (***Figure 4—figure supplement 1E–E''***). Reassuringly, *60H12-Gal4* > shi^{DN} animals do not show lethality on a control food diet (***Figure 4H***) allowing us to test rectal papillar physiological function on a high-salt diet. Using either pan-hindgut or papillae-specific knockdown of cytoplasm sharing regulators, we find both shi^{DN} and $ogre^{DN}$ animals are extremely sensitive to the high-salt diet (mean survival <1 day, ***Figure 4H***). These results underscore an important function for gap junction proteins, as well as membrane remodeling by Dynamin/Shibire, in cytoplasm sharing.

Discussion

A distinctive mechanism and model of cytoplasm sharing

Our findings identify *Drosophila* rectal papillae as a new and distinctive example of cytoplasm sharing between multiple nuclei in a simple, genetically tractable system. One defining property of papillar cytoplasm sharing is the lack of an easily observable conduit in the lateral membrane through

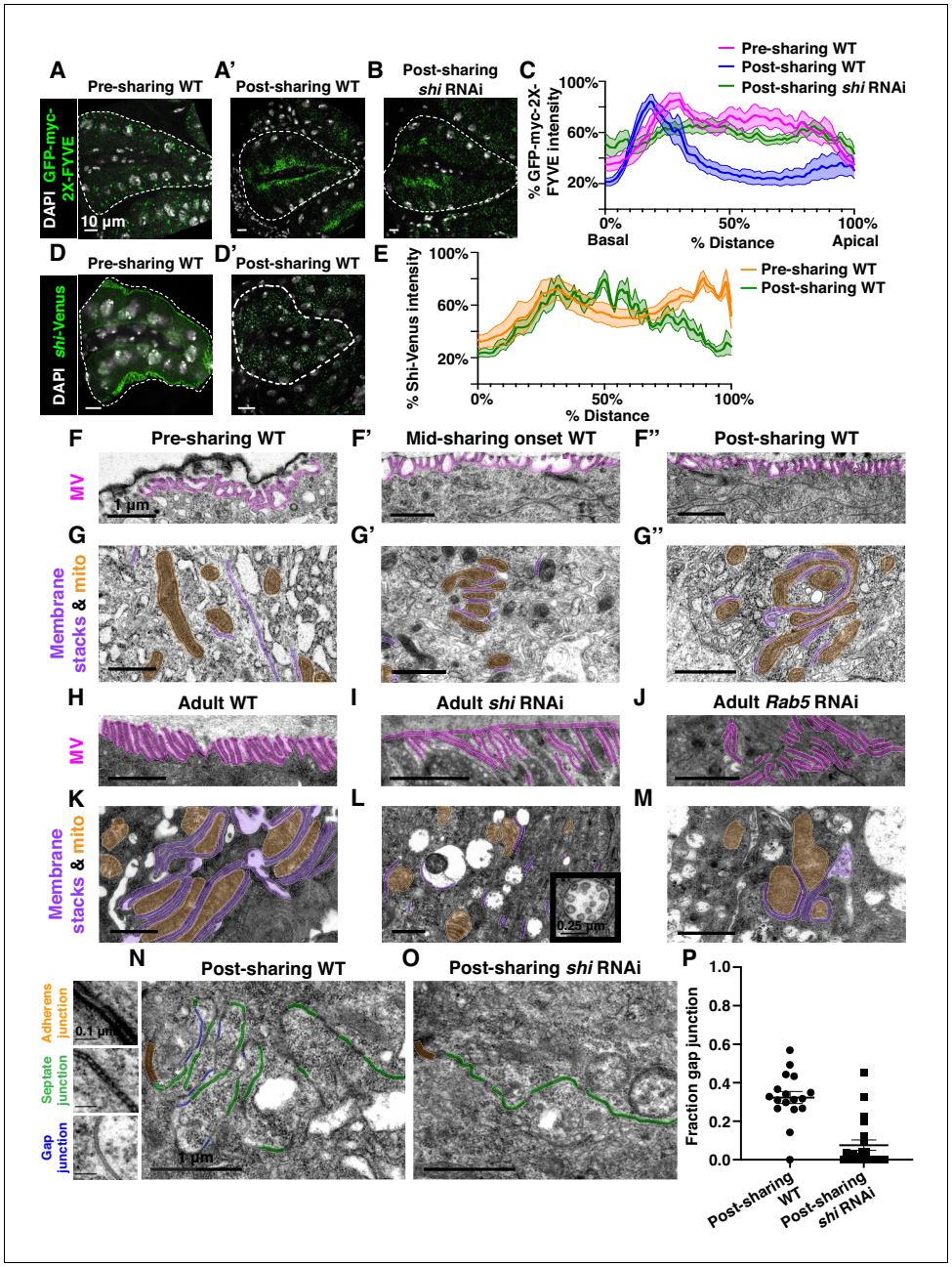

Figure 3. Gap junction establishment, but no membrane breaches, accompany cytoplasm sharing. (**A–A'**) Endosome localization (GFP-myc-2x-FYVE), representative of (**A**) pre- and (**A'**) post-sharing onset. (**B**) Endosomes in *shi RNAi* post-sharing, *see Methods*. (**C**) Aggregated endosome line profiles for WT pre-sharing (N = 6, rep = 3), WT post-sharing (N = 7, rep = 2), and *shi RNAi* post-sharing (N = 10, rep = 2). Shaded area represents standard error. (**D–D'**) Shi-Venus localization pre- and post-sharing onset. (**E**) Line profiles as in (**D–D'**) (N = 4–5, rep = 3). (**F–O**) Representative Transmission Electron Micrographs (TEMs). (**F–F''**) Microvillar-like structures (MV) pre- (**F**), mid- (**F'**), and post- (**F''**) sharing onset. (**G–G''**) Mitochondria and surrounding membrane pre- (**G**), mid- (**G'**), and post- (**G''**) sharing onset. (**H–J**) Microvillar-like structures (MV) of adult papillae in WT (**H**), *shi RNAi* (**I**), and *Rab5 RNAi* (**J**). (**K–M**) Mitochondria and surrounding membranes of adult papillae in WT (**K**), *shi RNAi* (**L**), and *Rab5 RNAi* (**M**). Inset in (**L**) shows trapped vesicles. (**N–O**) WT and *shi RNAi* post-sharing. Adherens (orange), septate (green), and gap (blue) junctions are highlighted. (**P**) Quantification of the ratio of gap junction length to septate plus gap junction length (Fraction gap junction) (N = 3–4, rep = 2). $p<0.0001$ for the difference in gap junction ratio between WT and *shi RNAi*.

The online version of this article includes the following figure supplement(s) for figure 3:

Figure 3 continued on next page

Figure 3 continued

Figure supplement 1. Changes in endosome polarity and apical junction shape accompany the onset of cytoplasm sharing.

Figure supplement 2. Extracellular spaces separate nuclei throughout much of the papillar lateral membrane.

which cytoplasm can be exchanged. Cytoplasm sharing in a multinucleate tissue/organism frequently involves the creation of a large membrane breach associated with major actin cytoskeleton rearrangement (***Kim et al., 2015***; ***Deng et al., 2017***; ***Martin, 2016***). However, papillar cytoplasm sharing does not require canonical myoblast fusion regulators nor major actin remodeling factors such as Rho family GTPases. Aside from membrane breaches, other cell types are known to share cytoplasm through the formation of cytoplasmic bridges such as ring canals or plasmodesmata. Such bridge structures assemble as the result of incomplete cytokinesis (***Mahowald, 1971***; ***Lůcas and Wolf, 1993***). In contrast, papillar cytoplasm sharing does not require mitosis or cytokinesis, and does not contain intercellular bridge structures visible by electron microscopy.

In addition to lacking a large, observable membrane breach, papillar cytoplasm sharing occurs within an intact, polarized epithelium, and apical cell–cell junctions and lateral membranes are retained after the onset of sharing. In contrast, other epithelia known to fuse cytoplasm, such as *C. elegans* epithelia fused by Epithelial Fusion Failure 1 (EFF-1), dismantle cell–cell junctions (***Smurova and Podbilewicz, 2016***). Further, cells with ring canals retain cell–cell junctions and lateral membranes (***Peifer et al., 1993***).

Given the retention of cell junctions and absence of clear intercellular bridges, channels, or breaches in lateral membrane, our data lead us to propose that a specialized function of gap junction proteins facilitates cytoplasm sharing between neighboring cells in an otherwise intact epithelium (***Figure 4I***). Although gap junctions typically transfer molecules of <1 kDa, elongated proteins up to 18 kDa are observed to pass through certain vertebrate gap junctions (***Cieniewicz and Woodruff, 2010***). Alternatively, gap junction-mediated cell to cell communication has been previously implicated in fusion of placental trophoblasts and osteoclasts (***Firth et al., 1980***; ***Dunk et al., 2012***; ***Schilling et al., 2008***), so we cannot rule out an indirect role for gap junctions in papillar cells, such as through regulation/recruitment of a fusogenic protein (***Petrany and Millay, 2019***). Future work beyond the scope of this study can determine if, for example, papillar gap junctions exhibit a specialized structure to directly facilitate exchange of large cytoplasmic contents. As for the connection between membrane remodeling and gap junction formation, Rab11 has been previously reported to recycle gap junction components in *Drosophila* brain and mammalian cell culture (***Augustin et al., 2017***). Dynamin2 was also implicated in gap junction plaque internalization in mammalian cells (***Gilleron et al., 2011***). However, neither of these factors has been previously implicated in gap junction establishment. We show that Dynamin is required for gap junction formation in papillar cells. Future studies will determine the exact role of Dynamin in gap junction establishment. Another clue for future study is that papillar cytoplasm sharing is developmentally regulated, occurring over a brief 6 hr window, and requires membrane remodeling by trafficking GTPases and gap junction establishment (***Figure 4I***, ***Figure 4—figure supplement 1H***). Our results argue that papillar sharing is triggered by a permanent structural rearrangement rather than an active transport mechanism, as the membrane remodelers we identified are required specifically during developmental membrane remodeling.

The mechanisms we report here may be relevant to other emerging roles for membrane remodeling and cytoplasm sharing in the literature. Here, we identify a close relationship between the formation of membrane stacks and cytoplasm sharing. Basolateral membrane infoldings to expand cellular surface area are a common feature of absorptive cells (***Pease, 1956***). The mammalian kidney tubule cells exhibit similar basolateral membrane extensions to which ion transporters such as the Na+/K+-ATPase are localized (***Maunsbach, 1966***; ***Molitoris et al., 1992***; ***Avner et al., 1992***; ***Pease, 1955***; ***Sjöstrand and Rhodin, 1953***). Our results suggest that the same membrane remodeling factors that regulate cytoplasm sharing are required for the formation of membrane stacks. To our knowledge, this is the first study to reveal factors involved in basolateral membrane infolding biogenesis. Additionally, our results may also explain other examples of cytoplasm sharing where the underlying mechanism remains to be determined, such as transient cytoplasm sharing in the zebrafish

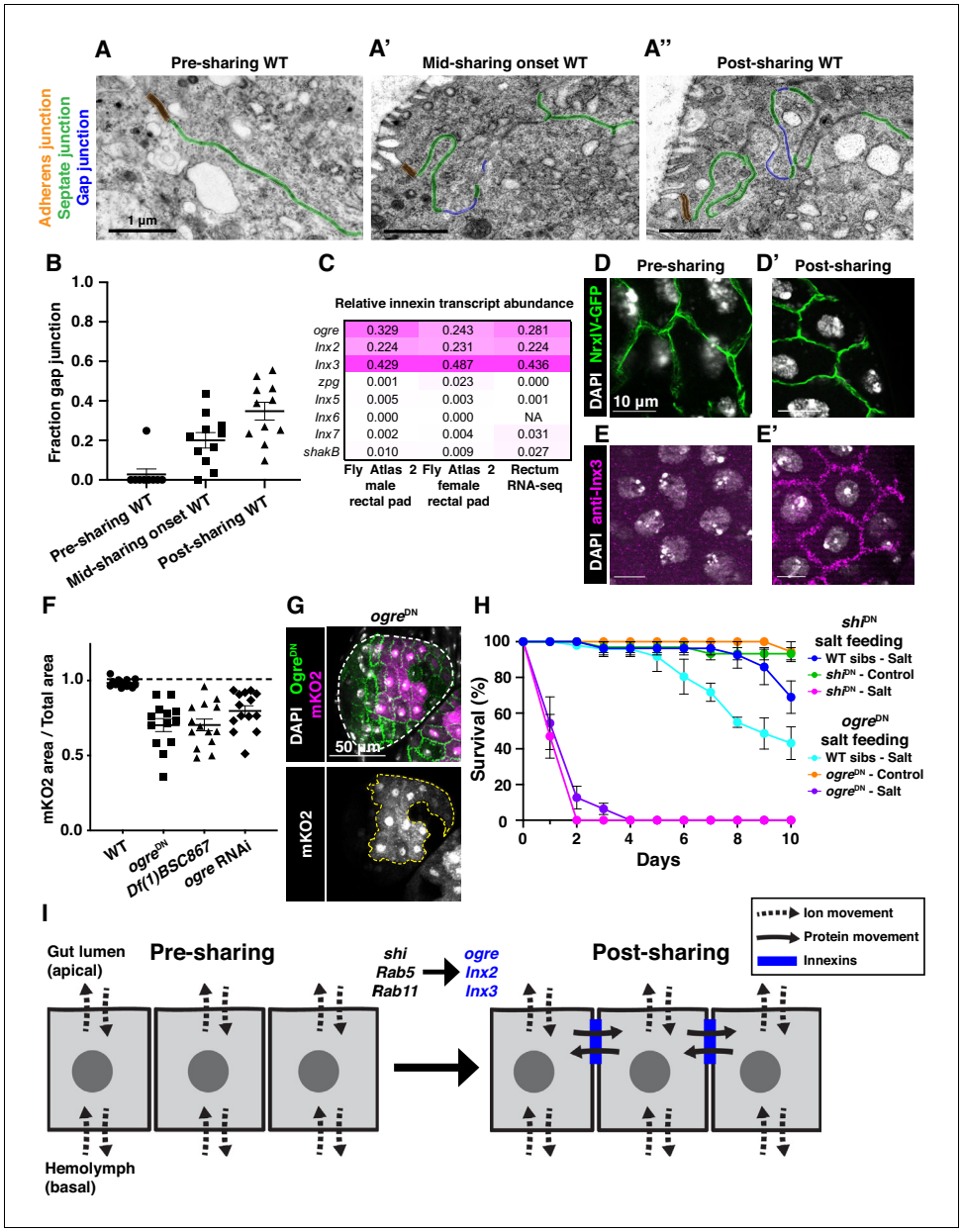

Figure 4. Gap junction proteins are required for cytoplasmic sharing. (**A–A''**) Representative apical junctions highlighted by junctional type in pre (**A**), mid (**A'**), and post (**A''**) sharing onset. (**B**) Quantification of fraction gap junction (gap junction length / (gap + septate junction length)) in pre-, mid-, and post-sharing onset pupae (N = 3–4, rep = 2). (**C**) *Drosophila* innexin expression in the adult rectum (*Methods*). (**D–D'**) Adherens junctions in pre- (**D**) and post- (**D'**) sharing pupae visualized by *NrxIV-GFP*. (**E–E'**) WT pupae pre- and post-sharing onset stained with anti-Inx3. (**F**) Quantification of cytoplasm sharing in WT, *ogre*^{DN}, *Df(1)BSC867/+* (a 10-gene-deficiency covering *ogre*, *Inx2*, and *Inx7*), and *ogre RNAi* adult papillae (N = 13–14, rep = 2). (**G**) Representative adult rectal papilla expressing *GFP-ogre* and *dBrainbow*. (**H**) Survival of WT, *shi*^{DN}, and *ogre*^{DN} animals on a high-salt diet (N = 27–37, rep = 3). (**I**) Proposed model for cytoplasmic sharing in an intact papillar epithelium.
The online version of this article includes the following figure supplement(s) for figure 4:

Figure supplement 1. Gap junction formation coincides with cytoplasm sharing onset.

myocardium (***Sawamiphak et al., 2017***). Together, our studies indicate that the *Drosophila* papillar epithelium represents a distinctive example of cytoplasmic sharing to generate giant multinucleate cells.

Functions and implications of transforming a multicellular tissue into a giant multinucleate cytoplasm

Our results have several implications for functions and regulation of multinucleation. Here we show that the membrane and junctional changes associated with cytoplasm sharing are required for normal *Drosophila* rectal papillar function. Papillae in other insects are known to undergo visible movement upon muscle contraction, which may facilitate cytoplasm movement (**Lowne, 1869**). Arthropod papillar structures are subject to peristaltic muscle contractions from an extensive musculature (**Rocco et al., 2017**), which aid in both excretion and movement of papillar contents into the hemolymph (**Habas mantel and Mantel, 1968**). Further, relative to other hindgut regions, the rectum appears to have specialized innervation (**Cohen et al., 2020**) and regulation by the kinin family of neuropeptides, which are hypothesized to provide additional input in to muscle activity in this critical site of reabsorption (**Audsley and Weaver, 2009**; **Lajevardi and Paluzzi, 2020**). We speculate that these muscle contractions aid in vigorous movement of papillar cytoplasm, which includes ions and water taken up from the intestinal lumen. The movement of these papillar contents may facilitate both cytoplasm exchange between papillar cells and the interaction of ions and ion transport machinery with intracellular membrane stacks. This idea is supported by our finding that animals lacking a large common papillar cytoplasm die when fed a high-salt diet.

Given the importance of insect papillae in pathogen biology, the knowledge that this common anatomical structure is a shared cytoplasm can impact both human disease intervention and agricultural pest control. Papillae occur in both primitive insect orders such as Zygentoma and Odonata and also in Lepidopterans, Hymenopterans, and Dipterans, the latter of which exhibit the most prominent and elaborate structures (**Palm, 1949**). Furthermore, electron micrographs of the hindgut of the mosquito, *Aedes aegypti*, and the ant, *Formica nigricans,* show striking ultrastructural similarity to *Drosophila*, and these studies leave open the possibility that multinucleation may be conserved in insect papillae (**Hopkins, 1967**; **Wessing and Eichelberg, 1973**; **Garayoa et al., 1999**). Cytoplasm sharing is a known mechanism that facilitates pathogen spread (**Eugenin et al., 2009**), and papillae are an avenue of entry for numerous pathogens including kinetoplastids and mosquito viruses (**Gu et al., 2010**; **Filosa et al., 2019**). Thus, our findings may impact strategies to prevent diseases such as African sleeping sickness, or to target agricultural pests that threaten agricultural production.

The sharing of cytoplasm also has the potential to neutralize detrimental genomic imbalances between nuclei caused by aneuploidy. Our prior work (**Schoenfelder et al., 2014**) revealed that papillae are highly tolerant of chromosome mis-segregation, and our work here suggests this tolerance may be due in part to neutralization of aneuploidies through cytoplasm sharing. This finding may also be relevant to the study of multinucleate tumors, such as those found in pancreas, bone, and fibrous tissues (**Doane et al., 2015**; **Hasegawa et al., 2017**; **Mancini et al., 2017**), or to conditions of aberrant organelle inheritance (**Asare et al., 2017**). Finally, we note that our study reveals that, even in a well-studied model organism such as *Drosophila,* we still have yet to appreciate the full diversity of tissue organization strategies. Our Brainbow-based approach could be applied to other contexts to identify other tissues with cytoplasm sharing, including those with gap junction-dependent but membrane breach-independent cytoplasm sharing. Collectively, our findings highlight the expanding diversity of multicellular tissue organization strategies.

Materials and methods

Key resources table

Reagent type (species) or resource	Designation	Source or reference	Identifiers	Additional information
Strain, strain background (*D. melanogaster*)	w^{1118}	Bloomington *Drosophila* Stock Center	BDSC:3605; FLYB:FBst0003605; RRID:BDSC_3605	w^{1118}
Genetic reagent (*D. melanogaster*)	*tub-Gal4*	Bloomington *Drosophila* Stock Center	BDSC:5138; FLYB:FBst0005138; RRID:BDSC_5138	y^1 w^*; P{tubP-GAL4} LL7/TM3, Sb^1 Ser^1

Continued on next page

Continued

Reagent type (species) or resource	Designation	Source or reference	Identifiers	Additional information
Genetic reagent (*D. melanogaster*)	*tub-Gal80^{ts}*	NA	NA	NA
Genetic reagent (*D. melanogaster*)	*UAS-dBrainbow*	Bloomington *Drosophila* Stock Center; (**Hampel et al., 2011**)	BDSC:34513; FLYB:FBst0034513; RRID:BDSC_34513	w^{1118}; P{UAS-Brainbow}attP2
Genetic reagent (*D. melanogaster*)	*UAS-dBrainbow*	Bloomington *Drosophila* Stock Center; (**Hampel et al., 2011**)	BDSC:34514; FLYB:FBst0034514; RRID:BDSC_34514	w^{1118}; P{UAS-Brainbow}attP40
Genetic reagent (*D. melanogaster*)	*Hsp70>cre*	Bloomington *Drosophila* Stock Center	BDSC:851; FLYB:FBst0000851; RRID:BDSC_851	y^{1} w^{67c23} P{Crey}1b; D*/TM3, Sb^{1}
Genetic reagent (*D. melanogaster*)	*UAS-fzr RNAi*	Vienna *Drosophila* Resource Center	VDRC:25550; FLYB:FBst0455950	w^{1118}; P{GD9960}v25550
Genetic reagent (*D. melanogaster*)	*UAS-shi RNAi #1*	Bloomington *Drosophila* Stock Center	BDSC:28513; FLYB:FBst0028513; RRID:BDSC_28513	y^{1} v^{1}; P{TRiP.JF03133}attP2
Genetic reagent (*D. melanogaster*)	*UAS-shi RNAi #2*	Bloomington *Drosophila* Stock Center	BDSC:36921; FLYB:FBst0036921; RRID:BDSC_36921	y^{1} sc* v^{1} sev^{21}; P{TRiP.HMS00154}attP2
Genetic reagent (*D. melanogaster*)	*UAS-Rab5 RNAi #1*	Bloomington *Drosophila* Stock Center	BDSC:30518; FLYB:FBst0030518; RRID:BDSC_30518	y^{1} v^{1}; P{TRiP.JF03335}attP2
Genetic reagent (*D. melanogaster*)	*UAS-Rab5 RNAi #2*	Bloomington *Drosophila* Stock Center	BDSC:67877; FLYB:FBst0067877; RRID:BDSC_67877	y^{1} sc* v^{1} sev^{21}; P{TRiP.GL01872}attP40
Genetic reagent (*D. melanogaster*)	*UAS-Rab11 RNAi #1*	Bloomington *Drosophila* Stock Center	BDSC:27730; FLYB:FBst0027730; RRID:BDSC_27730	y^{1} v^{1}; P{TRiP.JF02812}attP2
Genetic reagent (*D. melanogaster*)	*UAS-Rab11 RNAi #2*	Vienna *Drosophila* Resource Center	VDRC:22198; FLYB:FBst0454467	w^{1118}; P{GD11761}v22198
Genetic reagent (*D. melanogaster*)	*UAS-SCAR* RNAi #1	Bloomington *Drosophila* Stock Center	BDSC:36121; FLYB:FBst0036121; RRID:BDSC_36121	y^{1} sc* v^{1} sev^{21}; P{TRiP.HMS01536}attP40
Genetic reagent (*D. melanogaster*)	*UAS-SCAR RNAi #2*	Bloomington *Drosophila* Stock Center	BDSC:51803; FLYB:FBst0051803; RRID:BDSC_51803	y^{1} v^{1}; P{TRiP.HMC03361}attP40
Genetic reagent (*D. melanogaster*)	*UAS-kirre RNAi*	Vienna *Drosophila* Resource Center	VDRC:27227; FLYB:FBst0456824	w^{1118}; P{GD14476}v27227
Genetic reagent (*D. melanogaster*)	*UAS-sns RNAi*	Vienna *Drosophila* Resource Center	VDRC:877; FLYB:FBst0471238	w^{1118}; P{GD65}v877/TM3
Genetic reagent (*D. melanogaster*)	*UAS-schizo RNAi*	Vienna *Drosophila* Resource Center	VDRC:36625; FLYB:FBst0461775	w^{1118}; P{GD14895}v36625
Genetic reagent (*D. melanogaster*)	*UAS-sing RNAi*	Vienna *Drosophila* Resource Center	VDRC:12202; FLYB:FBst0450437	w^{1118}; P{GD3396}v12202/TM3
Genetic reagent (*D. melanogaster*)	*UAS-Cdc42^{DN}*	Bloomington *Drosophila* Stock Center	BDSC:6288; FLYB:FBst0006288; RRID:BDSC_6288	w*; P{UAS-Cdc42.N17}3

Continued on next page

Continued

Reagent type (species) or resource	Designation	Source or reference	Identifiers	Additional information
Genetic reagent (*D. melanogaster*)	*UAS-Rac1^{DN}*	Bloomington *Drosophila* Stock Center	BDSC:6292; FLYB:FBst0006292; RRID:BDSC_6292	y^{1} w*; P{UAS-Rac1.N17}1
Genetic reagent (*D. melanogaster*)	*UAS-Rho1^{DN}*	Bloomington *Drosophila* Stock Center	BDSC:7328; FLYB:FBst0007328; RRID:BDSC_7328	w*; P{UAS-Rho1.N19}2.1
Genetic reagent (*D. melanogaster*)	*UAS-GFP^{NLS}*	Bloomington *Drosophila* Stock Center	BDSC:4776; FLYB:FBst0004776; RRID:BDSC_4776	w^{1118}; P{UAS-GFP.nls}8
Genetic reagent (*D. melanogaster*)	*UAS-GFP-Myc-2x-FYVE*	Bloomington *Drosophila* Stock Center	BDSC:42712; FLYB:FBst0042712; RRID:BDSC_42712	w*; P{UAS-GFP-myc-2xFYVE}2
Genetic reagent (*D. melanogaster*)	*UAS-YFP-Rab5*	Bloomington *Drosophila* Stock Center	BDSC:9775; FLYB:FBst0009775; RRID:BDSC_9775	y^{1} w*; P{UASp-YFP.Rab5}Pde8^{08b}
Genetic reagent (*D. melanogaster*)	*60H12-Gal4*	Bloomington *Drosophila* Stock Center	BDSC:39268; FLYB:FBst0039268; RRID:BDSC_39268	w^{1118}; P{GMR60H12-GAL4}attP2
Genetic reagent (*D. melanogaster*)	*UAS-shi^{DN}*	Bloomington *Drosophila* Stock Center	BDSC:5822; FLYB:FBst0005822; RRID:BDSC_5822	w*; TM3, P{UAS-shi.K44A}3-10/TM6B, Tb^{1}
Genetic reagent (*D. melanogaster*)	*NrxIV-GFP*	Bloomington *Drosophila* Stock Center	BDSC:50798; FLYB:FBst0050798; RRID:BDSC_50798	y^{1} w*; P{PTT-GA}Nrx-IV^{CA06597}
Genetic reagent (*D. melanogaster*)	*Df(1)BSC867*	Bloomington *Drosophila* Stock Center	BDSC:29990; FLYB:FBst0029990; RRID:BDSC_29990	Df(1)BSC867, w^{1118}/Binsinscy
Genetic reagent (*D. melanogaster*)	*UAS-ogre RNAi*	Vienna *Drosophila* Resource Center	VDRC:7136; FLYB:FBst0470569	w^{1118}; P{GD3264}v7136
Genetic reagent (*D. melanogaster*)	*byn-Gal4*	**Singer et al., 1996**	FLYB:FBal0137290	P{GawB}byn^{Gal4}
Genetic reagent (*D. melanogaster*)	*UAS-GFP^{PA}*	Lynn Cooley; **McLean and Cooley, 2013**	FLYB:FBti0148163	P{20XUAS-IVS-Syn21-mC3PA-GFP-p10}
Genetic reagent (*D. melanogaster*)	*UAS-N^{DN}*	**Rebay et al., 1993**	NA	NA
Genetic reagent (*D. melanogaster*)	*UAS-shi-Venus*	Stefano De Renzis; **Fabrowski et al., 2013**	NA	NA
Genetic reagent (*D. melanogaster*)	*UAS-GFP-ogre*	Andrea Brand; **Spéder and Brand, 2014**	FLYB:FBtp0127574	ogre$^{UAS.N.GFP}$
Genetic reagent (*D. melanogaster*)	*UAS-Gapdh2-GFP^{PA}*	This paper	NA	Transgenic line created through gene synthesis and embryo injection. Codon-optimized *D. melanogaster* Gapdh2 fused to GFP^{PA}under UAS control.
Antibody	anti-GFP (Rabbit polyclonal)	Thermo Fisher Scientific	Cat# A11122; RRID:AB_221569	IF (1:1000)
Antibody	anti-HA (Rat monoclonal)	Roche	Cat# 11867423001; RRID:AB_390918	IF (1:100)

Continued on next page

Continued

Reagent type (species) or resource	Designation	Source or reference	Identifiers	Additional information
Antibody	anti-Inx3 (Rabbit polyclonal)	Reinhard Bauer; ***Lehmann et al., 2006***	RRID:AB_2568555	IF (1:75)
Antibody	Anti-Rabbit Alexa Fluor 488 (Goat)	Thermo Fisher Scientific	Cat# A32731; RRID:AB_2633280	IF (1:2000)
Antibody	Anti-Rabbit Alexa Fluor 568 (Goat)	Thermo Fisher Scientific	Cat# A-11011; RRID:AB_143157	IF (1:2000)
Antibody	Anti-Rat Alexa Fluor 633 (Goat)	Thermo Fisher Scientific	Cat# A-21094; RRID:AB_2535749	IF (1:2000)
Other	DAPI stain	Sigma-Aldrich	Cat# D9542	(1:5000)

Fly stocks and genetics

Flies were raised at 25˚C on standard media (Archon Scientific, Durham, NC) unless specified otherwise. See ***Table 4*** for a list of fly stocks used. See ***Table 3*** for a full list of fly lines screened in primary and secondary screens. See ***Table 5*** for panel-specific genotypes.

The *UAS-Gapdh2-GFP^{PA}* construct was generated by gene synthesis (Twist Biosciences). The GFP was placed at the C-terminus with a 12-amino acid fusion linker (GSAGSAAGSGEF) (***Waldo et al., 1999***) codon-optimized for *Drosophila*. This insert was then cloned into the pBID-UASC-FG vector modified to remove the FLAG tag and extraneous cloning sites. Transgenic flies were generated at Duke University. *brachyenteron (byn)-Gal4* was the driver for all UAS transgenes with the exception of the screen in ***Figure 1—figure supplement 1A***, which used *tub-Gal4*, and the *shi* knockdown in ***Figure 4H***, which used *60H12-Gal4. 60H12-Gal4* expresses only in the papillar cells and not the rest of the hindgut, and use of this driver blocks cytoplasm sharing using *UAS-shi^{DN}* (***Figure 4—figure supplement 1D–E''***). For all *Gal4* experiments, *UAS* expression was at 29˚C, except in ***Figure 1F–H***, where it was at 25˚C. If *byn-Gal4* expression of a given *UAS*-transgene was lethal, the experiment was repeated with a temperature-sensitive *Gal80^{ts}* repressor transgene and animals were kept at 18˚C until shifting to 29˚C at an experimentally-determined time point that would both result in viable animals and permit time to express the transgene prior to sharing onset.

For salt feeding assays, age- and sex-matched siblings were transferred into vials containing 2% NaCl food made with Nutri-Fly MF food base (Genesee Scientific) or control food (***Schoenfelder et al., 2014***). Flies were monitored for survival each day for 10 days.

Tissue preparation

For fixed imaging, tissues were dissected in PBS and immediately fixed in 3.7% formaldehyde + 0.3% Triton-X for 15 min. Immunostaining was performed in 0.3% Triton-X with 1% normal goat serum (***Fox et al., 2010***). The following antibodies were used: Rabbit anti-GFP (Thermo Fisher Scientific, Cat#A11122, 1:1000), Rat anti-HA (Roche, Cat#11867423001, 1:100), Rabbit anti-Inx3 (generous gift from Reinhard Bauer, 1:75), [***Lehmann et al., 2006***], 488, 568, 633 secondary antibodies (Thermo Fisher Scientific, Alexa Fluor, 1:2000). Tissue was stained with DAPI at 5 µg/ml and mounted in VECTASHIELD Mounting Media on slides.

Microscopy

Light microscopy

For fixed imaging, images were obtained on either a Leica SP5 inverted confocal with a 40X/1.25NA oil objective with emission from a 405 nm diode laser, a 488 nm argon laser, a 561 nm Diode laser, and a 633 HeNe laser under control of Leica LAS AF 2.6 software, or on an Andor Dragonfly Spinning Disk Confocal plus. Images were taken with two different cameras, iXon Life 888 1024 × 1024 EMCCD (pixel size 13 um) and the Andor Zyla PLUS 4.2 Megapixel sCMOS 2048 x 2048 (pixel size 6.5 um) depending on imaging needs. Images were taken on the **40x**/1.25–0.75 oil 11506250: 40X,

Table 3. Primary and secondary candidate screen stock numbers used and results.

Gene	Annotation symbol	Gene ID	Mutant or UAS transgene	Stock center	Stock number	Chr	Sharing disrupted?	Notes
Abi	CG9749	FBgn0020510	RNAi	BDSC	51455	2	No	
ALiX	CG12876	FBgn0086346	RNAi	BDSC	33417	3	No	
ALiX	CG12876	FBgn0086346	RNAi	BDSC	50904	2	No	
Arf51F	CG8156	FBgn0013750	RNAi	BDSC	51417	3	No	
Arf51F	CG8156	FBgn0013750	Mutant	BDSC	17076	2	No	
Arf51F	CG8156	FBgn0013750	RNAi	BDSC	27261	3	No	
Arp2	CG9901	FBgn0011742	RNAi	BDSC	27705	3	No	
Arp3	CG7558	FBgn0262716	RNAi	BDSC	32921	3	No	
Atg1	CG10967	FBgn0260945	RNAi	BDSC	44034	2	No	
Atg1	CG10967	FBgn0260945	RNAi	BDSC	26731	3	No	
Atg7	CG5489	FBgn0034366	RNAi	BDSC	34369	3	No	
Atg7	CG5489	FBgn0034366	RNAi	BDSC	27707	3	No	
Atg8a	CG32672	FBgn0052672	RNAi	BDSC	28989	3	No	
Atg8a	CG32672	FBgn0052672	RNAi	BDSC	58309	2	No	
Atg8a	CG32672	FBgn0052672	RNAi	BDSC	34340	3	No	
Atl	CG6668	FBgn0039213	RNAi	BDSC	36736	2	No	
Bet1	CG14084	FBgn0260857	RNAi	BDSC	41927	2	No	
blue	NA	FBgn0283709	RNAi	BDSC	44094	3	No	
blue	NA	FBgn0283709	RNAi	BDSC	41637	2	No	
CadN	CG7100	FBgn0015609	RNAi	BDSC	27503	3	No	
CadN	CG7100	FBgn0015609	RNAi	BDSC	41982	3	No	
CapD2	CG1911	FBgn0039680	Mutant	BDSC	59393	3	No	
Cdc2	CG5363	FBgn0004106	RNAi	VDRC	41838	3	Yes	
Cdc2	CG5363	FBgn0004106	RNAi	BDSC	NA	3	No	
Cdc42	CG12530	FBgn0010341	RNAi	BDSC	42861	2	No	
Cdc42	CG12530	FBgn0010341	DN	BDSC	6288	2	No	
Ced-12	CG5336	FBgn0032409	RNAi	BDSC	28556	3	No	
Ced-12	CG5336	FBgn0032409	RNAi	BDSC	58153	2	No	
Chc	CG9012	FBgn0000319	DN	BDSC	26821	2	No	
Chc	CG9012	FBgn0000319	RNAi	BDSC	27350	3	No	
Chc	CG9012	FBgn0000319	RNAi	BDSC	34742	3	No	
Chico	CG5686	FBgn0024248	RNAi	BDSC	36788	2	No	
Chmp1	CG4108	FBgn0036805	RNAi	BDSC	33928	3	No	
CHMP2B	CG4618	FBgn0035589	RNAi	BDSC	28531	3	No	
CHMP2B	CG4618	FBgn0035589	RNAi	BDSC	38375	2	No	
cindr	CG31012	FBgn0027598	RNAi	BDSC	35670	3	No	
cindr	CG31012	FBgn0027598	RNAi	BDSC	38976	2	No	
Clamp	CG1832	FBgn0032979	RNAi	BDSC	27080	3	No	
cno	CG42312	FBgn0259212	RNAi	BDSC	33367	3	No	
cno	CG42312	FBgn0259212	RNAi	BDSC	38194	2	No	
dac	CG4952	FBgn0005677	RNAi	BDSC	26758	3	No	
dac	CG4952	FBgn0005677	RNAi	BDSC	35022	3	No	
DCTN1-p150	CG9206	FBgn0001108	DN	BDSC	51645	2	No	

Table 3 continued on next page

Table 3 continued

Gene	Annotation symbol	Gene ID	Mutant or UAS transgene	Stock center	Stock number	Chr	Sharing disrupted?	Notes
dnd	CG6560	FBgn0038916	RNAi	BDSC	27488	3	No	
dnd	CG6560	FBgn0038916	RNAi	BDSC	34383	3	No	
dock	CG3727	FBgn0010583	RNAi	BDSC	27728	3	No	
dock	CG3727	FBgn0010583	RNAi	BDSC	43176	3	No	
dock	CG3727	FBgn0010583	Mutant	BDSC	11385	2	No	
Dr	CG1897	FBgn0000492	RNAi	BDSC	26224	3	No	
Dr	CG1897	FBgn0000492	RNAi	BDSC	42891	2	No	
Egfr	CG10079	FBgn0003731	DN	BDSC	5364	2	Yes	
Egfr	CG10079	FBgn0003731	RNAi	VDRC	43267	3	Yes	
endos	CG6513	FBgn0061515	RNAi	BDSC	53250	3	No	
endos	CG6513	FBgn0061515	RNAi	BDSC	65996	3	No	
Exo70	CG7127	FBgn0266667	RNAi	BDSC	28041	3	No	
Exo70	CG7127	FBgn0266667	RNAi	BDSC	55234	3	No	
Exo84	CG6095	FBgn0266668	RNAi	BDSC	28712	3	Yes	
Flo1	CG8200	FBgn0024754	RNAi	BDSC	36700	3	No	
Flo1	CG8200	FBgn0024754	RNAi	BDSC	36649	2	No	
Flo2	CG32593	FBgn0264078	RNAi	BDSC	55212	3	No	
Flo2	CG32593	FBgn0264078	RNAi	BDSC	40833	2	No	
fzr	CG3000	FBgn0262699	RNAi	VDRC	25550	2	Yes	
Gli	CG3903	FBgn0001987	RNAi	BDSC	31869	3	No	
Gli	CG3903	FBgn0001987	RNAi	BDSC	58115	2	No	
grk	CG17610	FBgn0001137	RNAi	BDSC	38913	3	No	
hbs	CG7449	FBgn0029082	RNAi	BDSC	57003	2	No	
Hem	CG5837	FBgn0011771	Mutant	BDSC	8752	3	No	
Hem	CG5837	FBgn0011771	Mutant	BDSC	8753	3	No	
Hem	CG5837	FBgn0011771	RNAi	BDSC	29406	3	No	
Hem	CG5837	FBgn0011771	RNAi	BDSC	41688	3	No	
Hsc70Cb	CG6603	FBgn0026418	RNAi	BDSC	33742	3	No	
Hsc70Cb	CG6603	FBgn0026418	DN	BDSC	56497	2	No	
Iris	CG4715	FBgn0031305	RNAi	BDSC	50587	2	No	
Iris	CG4715	FBgn0031305	RNAi	BDSC	63582	2	No	
l(2)gl	CG2671	FBgn0002121	RNAi	BDSC	31517	3	No	
lerp	CG31072	FBgn0051072	RNAi	BDSC	57436	2	No	
lilli	CG8817	FBgn0041111	RNAi	BDSC	26314	3	No	
lilli	CG8817	FBgn0041111	RNAi	BDSC	34592	3	No	
mbc	CG10379	FBgn0015513	RNAi	BDSC	32355	3	No	
mbc	CG10379	FBgn0015513	RNAi	BDSC	33722	3	No	
Mi-2	CG8103	FBgn0262519	RNAi	BDSC	16876	3	No	
mtm	CG9115	FBgn0025742	RNAi	BDSC	38339	3	No	
N	CG3936	FBgn0004647	DN	Rebay Lab	NA	2	No	
N	CG3936	FBgn0004647	RNAi	Sara Bray	NA	1	No	
Nrg	CG1634	FBgn0264975	RNAi	BDSC	28724	3	No	
Nrg	CG1634	FBgn0264975	RNAi	BDSC	38215	2	No	

Table 3 continued on next page

Table 3 continued

Gene	Annotation symbol	Gene ID	Mutant or UAS transgene	Stock center	Stock number	Chr	Sharing disrupted?	Notes
Nrg	CG1634	FBgn0264975	RNAi	BDSC	37496	2	No	
nrv3	CG8663	FBgn0032946	RNAi	BDSC	29431	3	No	
nrv3	CG8663	FBgn0032946	RNAi	BDSC	50725	3	No	
nuf	CG33991	FBgn0013718	RNAi	BDSC	31493	3	No	
pav	CG1258	FBgn0011692	RNAi	BDSC	35649	3	No	
pav	CG1258	FBgn0011692	RNAi	BDSC	43963	2	No	
Ptp61F	CG9181	FBgn0267487	RNAi	BDSC	32426	3	No	
Ptp61F	CG9181	FBgn0267487	RNAi	BDSC	56036	2	No	
Rab1	CG3320	FBgn0285937	CA	BDSC	9758	3	No	
Rab1	CG3320	FBgn0285937	DN	BDSC	9757	3	Yes	Requires 60H12-Gal4
Rab1	CG3320	FBgn0285937	RNAi	BDSC	27299	3	Yes	
Rab1	CG3320	FBgn0285937	RNAi	BDSC	34670	3	No	
Rab2	CG3269	FBgn0014009	CA	BDSC	9761	2	No	
Rab2	CG3269	FBgn0014009	DN	BDSC	9759	2	No	
Rab3	CG7576	FBgn0005586	CA	BDSC	9764	3	No	
Rab3	CG7576	FBgn0005586	DN	BDSC	9766	2	No	
Rab4	CG4921	FBgn0016701	CA	BDSC	9770	3	No	
Rab4	CG4921	FBgn0016701	DN	BDSC	9768	2	No	
Rab4	CG4921	FBgn0016701	DN	BDSC	9769	3	No	
Rab5	CG3664	FBgn0014010	CA	BDSC	9773	3	Yes	
Rab5	CG3664	FBgn0014010	DN	BDSC	42704	3	Yes	Requires 60H12-Gal4
Rab5	CG3664	FBgn0014010	RNAi	BDSC	67877	2	Yes	
Rab5	CG3664	FBgn0014010	RNAi	BDSC	30518	3	Yes	
Rab5	CG3664	FBgn0014010	RNAi	BDSC	51847	2	No	
Rab6	CG6601	FBgn0015797	CA	BDSC	9776	3	No	
Rab6	CG6601	FBgn0015797	DN	BDSC	23250	3	No	
Rab7	CG5915	FBgn0015795	CA	BDSC	9779	3	No	
Rab7	CG5915	FBgn0015795	DN	BDSC	9778	3	No	
Rab7	CG5915	FBgn0015795	DN	BDSC	9778	3	No	
Rab8	CG8287	FBgn0262518	DN	BDSC	9780	3	No	
Rab8	CG8287	FBgn0262518	CA	BDSC	9781	2	No	
Rab8	CG8287	FBgn0262518	DN	BDSC	9780	3	No	
Rab9	CG9994	FBgn0032782	CA	BDSC	9785	3	No	
Rab9	CG9994	FBgn0032782	DN	BDSC	23642	3	No	
Rab10	CG17060	FBgn0015789	CA	BDSC	9787	3	No	
Rab10	CG17060	FBgn0015789	DN	BDSC	9786	3	No	
Rab11	CG5771	FBgn0015790	CA	BDSC	9791	3	No	
Rab11	CG5771	FBgn0015790	DN	BDSC	23261	3	Yes	
Rab11	CG5771	FBgn0015790	RNAi	BDSC	27730	3	Yes	
Rab11	CG5771	FBgn0015790	RNAi	VDRC	108382	2	Yes	
Rab11	CG5771	FBgn0015790	RNAi	VDRC	22198	3	Yes	
Rab11	CG5771	FBgn0015790	Mutant	BDSC	42708	3	Yes	
Rab14	CG4212	FBgn0015791	CA	BDSC	9795	2	No	

Table 3 continued on next page

Table 3 continued

Gene	Annotation symbol	Gene ID	Mutant or UAS transgene	Stock center	Stock number	Chr	Sharing disrupted?	Notes
Rab14	CG4212	FBgn0015791	DN	BDSC	23264	3	No	
Rab18	CG3129	FBgn0015794	CA	BDSC	9797	3	No	
Rab18	CG3129	FBgn0015794	DN	BDSC	23238	3	No	
Rab19	CG7062	FBgn0015793	CA	BDSC	9800	3	No	
Rab19	CG7062	FBgn0015793	DN	BDSC	9799	3	No	
Rab21	CG17515	FBgn0039966	CA	BDSC	23864	2	No	
Rab21	CG17515	FBgn0039966	DN	BDSC	23240	3	No	
Rab23	CG2108	FBgn0037364	RNAi	BDSC	36091	3	No	
Rab23	CG2108	FBgn0037364	RNAi	BDSC	55352	2	No	
Rab23	CG2108	FBgn0037364	CA	BDSC	9806	3	No	
Rab23	CG2108	FBgn0037364	DN	BDSC	9804	3	No	
Rab26	CG34410	FBgn0086913	CA	BDSC	23243	3	No	
Rab26	CG34410	FBgn0086913	DN	BDSC	9808	3	No	
Rab27	CG14791	FBgn0025382	CA	BDSC	9811	2	No	
Rab27	CG14791	FBgn0025382	DN	BDSC	23267	2	No	
Rab30	CG9100	FBgn0031882	CA	BDSC	9814	2	No	
Rab30	CG9100	FBgn0031882	DN	BDSC	9813	3	No	
Rab32	CG8024	FBgn0002567	CA	BDSC	23280	3	No	
Rab32	CG8024	FBgn0002567	DN	BDSC	23281	2	No	
Rab35	CG9575	FBgn0031090	CA	BDSC	9817	3	No	
Rab35	CG9575	FBgn0031090	DN	BDSC	9820	3	No	
Rab39	CG12156	FBgn0029959	CA	BDSC	9823	3	No	
Rab39	CG12156	FBgn0029959	DN	BDSC	23247	3	No	
Rab40	CG1900	FBgn0030391	CA	BDSC	9827	3	No	
Rab40	CG1900	FBgn0030391	DN	BDSC	9829	2	No	
Rab9D	CG32678	FBgn0067052	CA	BDSC	9835	3	No	
Rab9D	CG32678	FBgn0067052	DN	BDSC	23257	2	No	
Rab9E	CG32673	FBgn0052673	CA	BDSC	9832	2	No	
Rab9E	CG32673	FBgn0052673	DN	BDSC	23255	3	No	
Rab9Fb	CG32670	FBgn0052670	CA	BDSC	9844	3	No	
Rab9Fb	CG32670	FBgn0052670	DN	BDSC	9845	2	No	
RabX1	CG3870	FBgn0015372	CA	BDSC	9839	2	No	
RabX1	CG3870	FBgn0015372	DN	BDSC	23252	3	No	
RabX2	CG2885	FBgn0030200	CA	BDSC	9842	3	No	
RabX2	CG2885	FBgn0030200	DN	BDSC	9843	2	No	
RabX4	CG31118	FBgn0051118	RNAi	BDSC	28704	3	No	
RabX4	CG31118	FBgn0051118	RNAi	BDSC	44070	2	No	
RabX4	CG31118	FBgn0051118	CA	BDSC	23277	2	No	
RabX4	CG31118	FBgn0051118	DN	BDSC	9849	3	No	
RabX5	CG7980	FBgn0035255	CA	BDSC	9852	X	No	
RabX5	CG7980	FBgn0035255	DN	BDSC	9853	2	No	
RabX6	CG12015	FBgn0035155	CA	BDSC	9855	2	No	
RabX6	CG12015	FBgn0035155	DN	BDSC	9856	3	No	

Table 3 continued on next page

Table 3 continued

Gene	Annotation symbol	Gene ID	Mutant or UAS transgene	Stock center	Stock number	Chr	Sharing disrupted?	Notes
CG41099	CG41099	FBgn0039955	RNAi	BDSC	34883	3	No	
Rac1	CG2248	FBgn0010333	RNAi	BDSC	28985	3	No	
Rac1	CG2248	FBgn0010333	DN	BDSC	6292	3	No	
Rala	CG2849	FBgn0015286	DN	BDSC	32094	2	No	
Rala	CG2849	FBgn0015286	RNAi	BDSC	34375	3	No	
Rbp9	CG3151	FBgn0010263	RNAi	BDSC	42796	3	No	
Rep	CG8432	FBgn0026378	RNAi	BDSC	28047	3	No	
rho	CG1004	FBgn0004635	Mutant	BDSC	1471	3	Yes	
rho	CG1004	FBgn0004635	RNAi	BDSC	38920	3	Yes	
rho	CG1004	FBgn0004635	RNAi	BDSC	41699	2	Yes	
Rho1	CG8416	FBgn0014020	DN	BDSC	7328	3	No	
Rho1	CG8416	FBgn0014020	DN	BDSC	58818	2	No	
Rho1	CG8416	FBgn0014020	RNAi	BDSC	32383	3	No	
Rip11	CG6606	FBgn0027335	RNAi	BDSC	38325	3	No	
rols	CG32096	FBgn0041096	RNAi	BDSC	56986	2	No	
rols	CG32096	FBgn0041096	RNAi	BDSC	58262	2	No	
rst	CG4125	FBgn0003285	RNAi	BDSC	28672	3	No	
ru	CG1214	FBgn0003295	RNAi	BDSC	41593	3	No	
ru	CG1214	FBgn0003295	RNAi	BDSC	58065	2	No	
SA-2	CG13916	FBgn0043865	RNAi	VDRC	108267	2	No	
SCAR	CG4636	FBgn0041781	RNAi	BDSC	31126	3	No	
SCAR	CG4636	FBgn0041781	RNAi	BDSC	51803	2	No	
SCAR	CG4636	FBgn0041781	Mutant	BDSC	8754	2	No	
sdt	CG32717	FBgn0261873	RNAi	BDSC	33909	3	No	
sdt	CG32717	FBgn0261873	RNAi	BDSC	35291	3	No	
Sec10	CG6159	FBgn0266673	RNAi	BDSC	27483	3	Yes	
Sec15	CG7034	FBgn0266674	RNAi	BDSC	27499	3	Yes	
Sec5	CG8843	FBgn0266670	RNAi	VDRC	28873	3	Yes	
Sec5	CG8843	FBgn0266670	RNAi	BDSC	50556	3	No	
Sec6	CG5341	FBgn0266671	RNAi	VDRC	105836	2	Yes	
Sec6	CG5341	FBgn0266671	RNAi	BDSC	27314	3	Yes	
Sec8	CG2095	FBgn0266672	RNAi	BDSC	57441	2	Yes	
shg	CG3722	FBgn0003391	RNAi	BDSC	27689	3	No	
shi	CG18102	FBgn0003392	DN	BDSC	5822	3	Yes	Requires 60H12-Gal4
shi	CG18102	FBgn0003392	RNAi	BDSC	28513	3	Yes	
shi	CG18102	FBgn0003392	RNAi	BDSC	36921	3	Yes	
siz	CG32434	FBgn0026179	RNAi	BDSC	39060	2	No	
spi	CG10334	FBgn0005672	RNAi	BDSC	28387	3	No	
spi	CG10334	FBgn0005672	RNAi	BDSC	34645	3	No	
stet	CG33166	FBgn0020248	RNAi	BDSC	57698	3	No	
Vha16-1	CG3161	FBgn0262736	RNAi	BDSC	40923	2	Yes	
Vha16-1	CG3161	FBgn0262736	RNAi	VDRC	104490	2	Yes	
Vha16-1	CG3161	FBgn0262736	RNAi	VDRC	49291	2	Yes	

Table 3 continued on next page

Table 3 continued

Gene	Annotation symbol	Gene ID	Mutant or UAS transgene	Stock center	Stock number	Chr	Sharing disrupted?	Notes
Vha16-2	CG32089	FBgn0028668	RNAi	BDSC	65167	2	No	
Vha16-3	CG32090	FBgn0028667	RNAi	BDSC	57474	2	No	
Vha16-5	CG6737	FBgn0032294	RNAi	BDSC	25803	3	Yes	
Vha55	CG17369	FBgn0005671	RNAi	BDSC	40884	2	No	
VhaAC39-1	CG2934	FBgn0285910	RNAi	BDSC	35029	3	No	
VhaAC39-2	CG4624	FBgn0039058	Mutant	BDSC	62725	3	No	
VhaAC39-2	CG4624	FBgn0039058	RNAi	VDRC	34303	2	No	
VhaPPA1-1	CG7007	FBgn0028662	RNAi	BDSC	57729	2	Yes	
VhaPPA1-2	CG7026	FBgn0262514	RNAi	BDSC	65217	2	Yes	
Vps2	CG14542	FBgn0039402	RNAi	VDRC	24869	3	Yes	
Vps2	CG14542	FBgn0039402	RNAi	BDSC	38995	2	Yes	
lsn	CG6637	FBgn0260940	RNAi	BDSC	38289	2	No	
Vps29	CG4764	FBgn0031310	RNAi	BDSC	53951	2	No	
Vps33b	CG5127	FBgn0039335	RNAi	BDSC	44006	2	No	
Vps35	CG5625	FBgn0034708	RNAi	BDSC	38944	2	No	
Vps4	CG6842	FBgn0283469	RNAi	BDSC	31751	3	No	
wts	CG12072	FBgn0011739	RNAi	BDSC	41899	3	No	
wash	CG13176	FBgn0033692	RNAi	BDSC	62866	2	No	
WASp	CG1520	FBgn0024273	RNAi	BDSC	25955	3	No	
WASp	CG1520	FBgn0024273	RNAi	BDSC	51802	2	No	
βggt-II	CG18627	FBgn0028970	RNAi	BDSC	50516	2	No	
βggt-II	CG18627	FBgn0028970	RNAi	BDSC	34902	3	No	

HCX PL APO, NA: 1.25, Oil, DIC, WD: 0.1 mm, coverglass: 0.17 mm, Iris diaphragm, Thread type: M25, **63x**/1.20 water 11506279: 63X, HCX PL APO W Corr CS, NA: 1.2, Water, DIC, WD: 0.22 mm, Coverglass: 0.14–0.18mm, thread type: M25, and **100x**/1.4–0.70 oil 11506210: HCX PL APO, NA: 1.4, Oil, DIC, WD: 0.09 mm, Coverglass: 0.17 mm, Iris Diaphragm, Thread type: M25. The lasers used were: 405 nm diode laser, 488 nm argon laser, 561 nm diode laser, and HeNe 633 nm laser.

For live imaging, hindguts were dissected and cultured based on previous protocols (***Fox et al., 2010***). Live imaging of cell fusion was performed on a spinning disc confocal (Yokogawa CSU10 scanhead) on an Olympus IX-70 inverted microscope using a 40x/1.3 NA UPlanFl N Oil objective, a 488 nm and 568 nm Kr-Ar laser lines for excitation and an Andor Ixon3 897 512 EMCCD camera. The system was controlled by MetaMorph 7.7.

Photo-activation was carried out using Leica SP5 and SP8 microscopes and the FRAP Wizard embedded in the Leica AS-F program. An initial z-stack of the tissue was acquired both before and after activation to examine the full extent of GFP^{PA} movement in three dimensions. GFP^{PA} transgenes were activated by either point activation or region of interest activation with the 405 nm laser set to between 5 and 20%, depending on the microscope and sample of interest. For each imaging session, test activations on nearby tissues were performed prior to quantify experiments to ensure that only single cells were being activated. After activation, the wizard software was used to acquire time lapses of 15 s to 2min of a single activation plane in order to capture protein movement. Extremely low 488 nm and 405 nm laser powers were used in acquisition of the time lapse images of GFP and Hoechst respectively. Low level 405 nm scanning did not significantly activate GFP^{PA}, and control experiments were performed without the use of 405 nm time lapses and showed the same protein movement results (data not shown).

Table 4. Fly stocks used in addition to the screens.

Stock name	Stock number	Origin	References
w^{1118}	3605	BDSC	
tub-Gal4	5138	BDSC	
tub-Gal80^{ts}	NA	NA	
UAS-dBrainbow	34513	BDSC	**Hampel et al., 2011**
UAS-dBrainbow	34514	BDSC	**Hampel et al., 2011**
Hsp70 > cre	851	BDSC	
UAS-fzr RNAi	25550	VDRC	**Fox et al., 2010**; **Schoenfelder et al., 2014**
UAS-shi RNAi #1	28513	BDSC	
UAS-shi RNAi #2	36921	BDSC	
UAS-Rab5 RNAi #1	30518	BDSC	
UAS-Rab5 RNAi #2	67877	BDSC	
UAS-Rab11 RNAi #1	27730	BDSC	
UAS-Rab11 RNAi #2	22198	VDRC	
UAS-SCAR RNAi #1	36121	BDSC	**Bischoff et al., 2013**
UAS-SCAR RNAi #2	51803	BDSC	**Xing et al., 2018**
UAS-kirre RNAi	27227	VDRC	**Linneweber et al., 2015**
UAS-sns RNAi	877	VDRC	**Linneweber et al., 2015**
UAS-schizo RNAi	36625	VDRC	**Johnson et al., 2011**
UAS-sing RNAi	12202	VDRC	**Brunetti et al., 2015**
UAS-Cdc42^{DN}	6288	BDSC	
UAS-Rac1^{DN}	6292	BDSC	
UAS-Rho1^{DN}	7328	BDSC	
UAS-GFP^{NLS}	4776	BDSC	
UAS-GFP-Myc-2x-FYVE	42712	BDSC	**Gillooly et al., 2000**; **Wucherpfennig et al., 2003**
UAS-YFP-Rab5	9775	BDSC	
60H12-Gal4	39268	BDSC	
UAS-shi^{DN}	5822	BDSC	
NrxIV-GFP	50798	BDSC	
Df(1)BSC867	29990	BDSC	
UAS-ogre RNAi	7136	VDRC	**Holcroft et al., 2013**; **Spéder and Brand, 2014**
byn-Gal4	-	NA	**Singer et al., 1996**
UAS-GFP^{PA}	-	Lynn Cooley	**Datta et al., 2008**
UAS-N^{DN}	-	NA	**Rebay et al., 1993**
UAS-shi-Venus	-	Stefano De Renzis	**Fabrowski et al., 2013**
UAS-GFP-ogre	-	Andrea Brand	**Spéder and Brand, 2014**
UAS-Gapdh2-GFP^{PA}	-	-	This paper

Transmission electron microscopy

Hindguts were dissected into PBS and fixed in a solution of 2.5% glutaraldehyde in 0.1% cacodylate buffer, pH 7.2. Post-fix specimens were stained with 1% osmium tetroxide in 0.1M cacodylate buffer, dehydrated, soaked in a 1:1 propylene oxide:Epon 812 resin, and then embedded in molds with fresh Epon 812 resin at 65˚C overnight. The blocks were cut into semi-thin (0.5 µm) sections using Leica Reichert Ultracuts and the sections were stained with 1% methylene blue. After inspection,

Table 5. Additional Methods.

Panel	Additional methods
Figure 1—figure supplement 1F-F''	*Hsp70 > cre; UAS-dBrainbow; byn-Gal4* papillae dissected at 62 (D), 69 (D'), or 80 (D'') hours post-puparium formation (HPPF) at 25˚C. Hindguts were stained with Rabbit anti-GFP (Thermo-Fisher, A11122, 1:1000), Rat anti-HA (Sigma, 3F10, 1:100), and DAPI at 5 µg/ml.
Figure 1G	*Hsp70 > cre; UAS-dBrainbow; byn-Gal4* papillae dissected at various HPPF at 25˚C. The area labeled by mKO2 was divided by total papillar area.
Figure 1H	*Hsp70 > cre; UAS-dBrainbow; byn-Gal4* papillae live-imaged at 69HPPF at 25˚C.
Figure 1H'	Fluorescence intensity measured in neighboring cells during sharing onset (1H).
Figure 1I-I'	*byn-Gal4/UAS-GFP^{PA}*, live-imaged during adulthood. Single secondary and principal cells were photoactivated and imaged every 3 s.
Figure 2A	UAS-RNAis and dominant-negative versions of 77 genes representing a wide range of cellular roles were screened (*Hsp70 > cre*; *UAS-dBrainbow*; *byn-Gal4*) for sharing defects. Animals expressing both *UAS-dBrainbow* and an *UAS*-driven RNAi or mutant gene were raised at 25˚C and shifted to 29˚C at L3. If a given RNAi or DN line was lethal when expressed with the *byn-Gal4* driver, a *Gal80^{ts}* was crossed in and the animals raised at 18˚C with a shift to 29˚C at pupation. Given the robustness of cytoplasmic sharing in WT animals, gene knockdowns or mutants with even single cell defects in sharing were considered 'hits'.
Figure 2B	Secondary screen of 36 genes representing various categories of membrane trafficking (*Hsp70 > cre*; *UAS-dBrainbow*; *byn-Gal4*) for sharing defects. Animals expressing both *UAS-dBrainbow* and an *UAS*-driven RNAi were raised at 25˚C and shifted to 29˚C at L3. If a given RNAi line was lethal when expressed with the *byn-Gal4* driver, a *Gal80^{ts}* was crossed in and the animals raised at 18˚C with a shift to 29˚C at pupation. Given the robustness of cytoplasmic sharing in WT animals, gene knockdowns with even single cell defects in sharing were considered 'hits'.
Figure 2C	Secondary screen (*Hsp70 > cre*; *UAS-dBrainbow*; *byn-Gal4*) of dominant-negative and constitutively-active variants of the Drosophila Rab GTPases. *UAS-Rab11^{DN}* and *UAS-Rab14^{DN}* required a *Gal80^{ts}* repressor and temperature shifts from 18 to 29˚C at pupation. *UAS-Rab1^{DN}* and *UAS-Rab5^{DN}* required papillar-specific expression using an alternative *Gal4* driver (*60* H12-Gal4), *Gal80^{ts}* repressor, and temperature shifts from 18 to 29˚C at pupation.
Figure 2D	*Hsp70 > cre*; *UAS-dBrainbow*; *byn-Gal4, Gal80^{ts}* animals dissected pre-sharing (48 HPPF at 29˚C).
Figure 2D'	*Hsp70 > cre*; *UAS-dBrainbow*; *byn-Gal4, Gal80^{ts}* animals raised at 18˚C and shifted to 29˚C at pupation and dissected post-sharing (young adult).
Figure 2E	Young adult animals expressing *UAS-shi RNAi #1* in a *Hsp70 > cre*; *UAS-dBrainbow*; *byn-Gal4, Gal80^{ts}* background. Animals were shifted from 18 to 29˚C at pupation to maximize RNAi and minimize animal lethality.
Figure 2F	Young adult animals expressing *UAS-Rab5 RNAi #1* in a *Hsp70 > cre*; *UAS-dBrainbow*; *byn-Gal4, Gal80^{ts}* background. Animals were shifted from 18 to 29˚C at 1–2 days PPF to maximize RNAi and minimize animal lethality.
Figure 2G	Young adult animals expressing *UAS-Rab11 RNAi #2* in a *Hsp70 > cre*; *UAS-dBrainbow*; *byn-Gal4, Gal80^{ts}* background. Animals were shifted from 18 to 29˚C at 1–2 days PPF to maximize RNAi and minimize animal lethality.
Figure 2H	Animals were shifted and dissected as in 2D-G. Additionally, *Hsp70 > cre*; *UAS-dBrainbow*; *byn-Gal4, Gal80^{ts}* animals expressing *UAS-shi RNAi #2* were raised at 18˚C and shifted to 29˚C at pupation, animals expressing *UAS-Rab5 RNAi #2* were raised at 18˚C and shifted to 29˚C at L3, and animals expressing *UAS-Rab11 RNAi #1* were raised at 18˚C and shifted to 29˚C at 1–2 days PPF.
Figure 3A-A'	Pupae expressing the early and late endosome marker *UAS-GFP-myc-2x-FYVE* were dissected pre (A, 48HPPF at 29˚C) and post (A', 72HPPF at 29˚C) sharing onset.
Figure 3B	Pupae expressing *UAS-GFP-myc-2x-FYVE* in a *UAS-shi RNAi #1* background at a post-sharing time point (24HPPF at 18˚C + 72 hr at 29˚C).
Figure 3C	Aggregated line profiles of *UAS-GFP-myc-2x-FYVE* intensity across papilla.
Figure 3D-D'	Pupae expressing *UAS-shi-Venus* were dissected pre (D, 48HPPF at 29˚C) and post (D', 72HPPF at 29˚C) sharing onset.
Figure 3E	Aggregated line profiles of Shi-Venus intensity from the basal (0% distance) to the apical (100% distance) edges of the papilla. See 3C.
Figure 3F-F''	Transmission electron micrographs of the microvillar-like structures of pupal papillae pre (F, 60HPPF at 25˚C), mid (F', 66HPPF at 25˚C), and post (F'', 69HPPF at 25˚C) cytoplasm sharing onset.
Figure 3G-G''	Electron micrographs of mitochondria and surrounding membrane material pre (G, 60HPPF at 25˚C), mid (G', 66HPPF at 25˚C), and post (G'', 69HPPF at 25˚C)
Figure 3H	Electron micrograph of microvillar-like structures of WT (*w^{1118}*) young adult papillar cells.
Figure 3I	Electron micrograph of microvillar-like structures of young adult *byn-Gal4, Gal80^{ts}*, *UAS-shi RNAi #2* (raised at 18˚C, shifted at pupation to 29˚C).
Figure 3J	Electron micrograph of microvillar-like structures of young adult *byn-Gal4, Gal80^{ts}*, *UAS-Rab5 RNAi #1* animals (raised at 18˚C, shifted at 1–2 days PPF to 29˚C).
Figure 3K	Electron micrograph of mitochondria and surrounding membrane material of WT (*w^{1118}*) young adult papillar cells.
Figure 3L	Electron micrograph of mitochondria and surrounding membrane material of young adult *byn-Gal4, Gal80^{ts}*, *UAS-shi RNAi #2* (raised at 18˚C, shifted at pupation to 29˚C).

Table 5 continued on next page

Table 5 continued

Panel	Additional methods
Figure 3M	Electron micrograph of mitochondria and surrounding membrane material of young adult *byn-Gal4, Gal80^{ts}, UAS-Rab5 RNAi #1* animals (raised at 18˚C, shifted at 1–2 days PPF to 29˚C).
Figure 3N	Electron micrograph of post-sharing WT (TM3/*UAS-shi RNAi #1*) pupa (24HPPF at 18˚C, shifted to 29˚C for 50 hr, then dissected)
Figure 3O	Electron micrograph of post-sharing *byn-Gal4, Gal80^{ts},UAS-shi RNAi #1* pupa (24HPPF at 18˚C, shifted to 29˚C for 50 hr, then dissected)
Figure 3P	Gap junction length / (gap junction length + septate junction length) measured in WT and *UAS-shi RNAi #1* pupae (see 3N-3O). Each point represents an image of a junction.
Figure 4A-A''	Electron micrographs of apical junctions (adherens, septate, and gap) pre (A, 60HPPF at 25˚C), mid (A', 66HPPF at 25˚C), and post (A'', 69HPPF at 25˚C)
Figure 4B	Gap junction length / (gap junction length + septate junction length) measured in pupae pre (60HPPF at 25˚C), mid (66HPPF at 25˚C), and post (69HPPF at 25˚C) sharing onset. Each point represents an image of a junction.
Figure 4C	Relative innexin transcript abundance (innexin X transcripts/total innexin transcripts) using data from Fly Atlas 2 (***Leader et al., 2018***) and RNA-seq of adult *w^{1118}* rectums performed in the Fox Lab.
Figure 4D-D'	Pupae with endogenously GFP-tagged NrxIV (*NrxIV-GFP*) dissected pre (D, 48HPPF) and post (D', 72HPPF) sharing onset.
Figure 4E-E'	Pupae stained with Inx3 antibody (gift from Reinhard Bauer, rabbit, 1:75) pre (E, 48HPPF) and post (E', 58HPPF, papillae do not stain well at later timepoints) sharing onset.
Figure 4F	Young adult animals expressing no transgene (WT), *UAS-ogre^{DN}*, *UAS-ogre RNAi*, or containing a deficiency covering *ogre*, *Inx2*, and *Inx7* in a *Hsp70 > cre; UAS-dBrainbow; byn-Gal4, Gal80^{ts}* background. Animals were raised at 25˚C until L3 and then shifted to 29˚C until dissection at young adulthood.
Figure 4G	See ***Figure 4F***.
Figure 4H	*60* H12-Gal4, *Gal80^{ts}* driving *UAS-shi^{DN}* and WT siblings were shifted from 18 to 29˚C at pupation. *byn-Gal4, Gal80^{ts}* driving *UAS-ogre^{DN}* animals and WT siblings were raised at 25˚C and shifted to 29˚C at L3. Animals 1–3 days post-eclosion were sorted into sex-matched groups and fed a control diet or a high salt (2% NaCl) diet. Survival was assessed once per day for 10 days.
Figure 1—figure supplement 1A	*Hsp70 > cre; UAS-dBrainbow; tubulin-Gal4* animals raised at 29˚C. Tissues dissected at adulthood.
Figure 1—figure supplement 1D	*byn-Gal4/UAS-Gapdh2-GFP^{PA}* raised at 29˚C and live-imaged during adulthood. Principal cells were photoactivated and imaged every 15 s.
Figure 1—figure supplement 1E	*Hsp70 > cre*; UAS-*dBrainbow*; *byn-Gal4* animals were shifted from 25 to 29˚C during L3 and dissected at adulthood.
Figure 1—figure supplement 1F	*Hsp70 > cre*; UAS-*dBrainbow/UAS-fzr RNAi*; *byn-Gal4* animals were shifted from 25 to 29˚C during L2 to maximize *fzr* knock down during endocycling. Animals were dissected at adulthood.
Figure 1—figure supplement 1G	*Hsp70 > cre; UAS-dBrainbow; byn-Gal4/UAS-N^{DN}* animals were shifted from 25 to 29˚C during L3 to ensure maximum *UAS-N^{DN}* expression during mitoses. Animals were dissected at adulthood.
Figure 2—figure supplement 1A	*Hsp70 > cre*; *UAS-dBrainbow*; *byn-Gal4, Gal80^{ts}* animals expressing various previously published myoblast fusion RNAis raised at 25˚C and shifted to 29˚C at L3 and dissected post-sharing (young adult).
Figure 2—figure supplement 1B	*Hsp70 > cre*; *UAS-dBrainbow*; *byn-Gal4, Gal80^{ts}* animals expressing various previously published UAS-dominant-negative active regulators raised at 18˚C and shifted to 29˚C at L3 and dissected post-sharing (young adult).
Figure 2—figure supplement 1C	Papillar cells were identified using *byn-Gal4, Gal80^{ts}*, driving *UAS-GFP^{NLS}* expression. Cells were counted in one, z-sectioned half of the papillae and multiplied by two to give an approximate cell count.
Figure 2—figure supplement 1D	*Hsp70 > cre*; *UAS-dBrainbow*; *byn-Gal4, Gal80^{ts}* animals were raised at 18˚C until 3–4 days PPF and shifted to 29˚C and dissected at young adulthood.
Figure 2—figure supplement 1E	*Hsp70 > cre*; *UAS-dBrainbow*; *byn-Gal4, Gal80^{ts}* animals expressing *UAS-shi RNAi #1* were raised at 18˚C until 3–4 days PPF and shifted to 29˚C and dissected at young adulthood.
Figure 3—figure supplement 1A	See ***Figure 3A-C***. Basal and apical membrane defined as 10–20% and 90–100% total distance of papillae, respectively.
Figure 3—figure supplement 1B-B'	*byn-Gal4 > UAS-Rab5-YFP* animals dissected pre (48HPPF, 29˚C) and post (72HPPF, 29˚C) sharing onset.
Figure 3—figure supplement 1B''	See ***Figure 3—figure supplement 1B-B'*** and ***Figure 3C***.
Figure 3—figure supplement 1C-C''	Electron micrographs of apical junctions (adherens, septate, and gap) pre (D, 60HPPF at 25˚C), mid (D', 66HPPF at 25˚C), and post (D'', 69HPPF at 25˚C)
Figure 3—figure supplement 1D	Electron micrograph of apical junctions (adherens, septate, and gap) of WT (*w^{1118}*) young adult papillar cells.

Table 5 continued on next page

Table 5 continued

Panel	Additional methods
Figure 3—figure supplement 1E	Electron micrograph of apical junctions (adherens, septate, and gap) of young adult *byn-Gal4, Gal80^{ts}*ts, *UAS-shi RNAi #2* (raised at 18˚C, shifted at pupation to 29˚C).
Figure 3—figure supplement 1F	Electron micrograph of apical junctions (adherens, septate, and gap) of young adult *byn-Gal4, Gal80^{ts}*ts, *UAS-Rab5 RNAi #1* animals (raised at 18˚C, shifted at 1–2 days PPF to 29˚C).
Figure 3—figure supplement 1G	See ***Figure 3N-O***. Junction width was measured throughout and averaged per image. Each point represents one image of a junction.
Figure 3—figure supplement 1G'	See ***Figure 3N-O***. Junction width was measured throughout and averaged per image. Each point represents one image of a junction.
Figure 3—figure supplement 1G''	See ***Figure 3N-O***. Raw lengths shown were used to calculate 'fraction gap junction' in 3P. Each point represent one image of a junction.
Figure 3—figure supplement 2A	TEM of young adult (*w^{1118}*) papilla.
Figure 4—figure supplement 1A	See ***Figure 4A-B***. Junction width was measured throughout and averaged per image. Each point represents one image of a junction.
Figure 4—figure supplement 1A'	See ***Figure 4A-B***. Junction width was measured throughout and averaged per image. Each point represents one image of a junction.
Figure 4—figure supplement 1A''	See ***Figure 4A-B***. Raw lengths shown were used to calculate 'fraction gap junction' in 3P. Each point represent one image of a junction.
Figure 4—figure supplement 1B-B'	Pupae expressing *byn-Gal4, Gal80^{ts}*ts, *UAS-ogre^{DN}* (*UAS-GFP-ogre*) dissected pre (B, 48HPPF, 29˚C) and post (B', 72HPPF, 29˚C) sharing onset.
Figure 4—figure supplement 1C	*byn-Gal4, Gal80^{ts}* pupae raised at 18˚C until 0HPPF and then shifted to 29˚C until dissection at 58HPPF. Pupal rectums were stained with Inx3 antibody (gift from Reinhard Bauer, rabbit, 1:75).
Figure 4—figure supplement 1C'	*byn-Gal4, Gal80^{ts}*ts, *UAS-shi RNAi #2* pupae raised at 18˚C until 0HPPF and then shifted to 29˚C until dissection at 58HPPF. Pupal rectums were stained with Inx3 antibody (gift from Reinhard Bauer, rabbit, 1:75).
Figure 4—figure supplement 1D	*byn-Gal4 > UAS-GFP^{NLS}* dissected pre (48HPPF, 29˚C) sharing onset.
Figure 4—figure supplement 1D'	*60H12-Gal4 > UAS-GFP^{NLS}* dissected pre (48HPPF, 29˚C) sharing onset. The pan-hindgut driver used in previous experiments, *brachyenteron* (*byn-Gal4*), causes animal lethality with *shi*, *Rab5*, and *Rab11* knockdown within a few days. We therefore screened for and identified an alternative, papillae-specific driver (*60H12-Gal4*), derived from regulatory sequences of the hormone receptor gene *Proctolin Receptor*. *60H12-Gal4 > shi^{DN}* animals are viable on a control diet allowing us to test papillar function on a high-salt diet.
Figure 4—figure supplement 1E	*Hsp70 > cre; UAS-dBrainbow; 60H12-Gal4* animals raised at 18˚C and shifted to 29˚C at pupation and dissected as young adults.
Figure 4—figure supplement 1E'	*Hsp70 > cre; UAS-dBrainbow; 60H12-Gal4 / UAS-shi^{DN}* animals raised at 18˚C and shifted to 29˚C at pupation and dissected as young adults.
Figure 4—figure supplement 1E''	See ***Figure 4—figure supplement 1E-E'***.

ultra-thin sections (65−75 nm) were cut using Leica EM CU7 and contrast stained with 2% uranyl acetate, 3.5% lead citrate solution. Ultrathin sections were visualized on a JEM-1400 transmission electron microscope (JEOL) using an ORIUS (1000) CCD 35 mm port camera.

Image analysis

All image analysis was performed using ImageJ and FIJI (***Rueden et al., 2017***; ***Schindelin et al., 2012***).

Cytoplasm sharing calculation

Cytoplasmic sharing was quantified by manually tracing the total papillar area by morphology and the area marked by mKO2 signal in one z-slice of the papillar face of each animal. The area marked by mKO2 was summed and divided by the sum of the total papillar area to yield the papillar fraction marked by mKO2 which indicates the degree of cytoplasmic sharing within each animal. Papillae without mKO2 signal were excluded from the area measurements.

Table 6. Additional statistics.

Panel	N (animals) per group	Bio. reps	Statistical test	P-value
Figure 1G	9–18	2	Unpaired t-test	66HPPF:74HPPF < 0.0001
Figure 2H	9–32	2–3	One-way ANOVA with Tukey's multiple comparisons test	ANOVA:<0.0001 Pre:WT < 0.0001 WT:*shi #1* < 0.0001 WT:*shi #2* < 0.0001 WT:*Rab5 #1* < 0.0001 WT:*Rab5 #2* < 0.0001 WT:*Rab11 #1* < 0.0001 WT:*Rab11 #2* < 0.0001 *shi #1*:*Rab5 #2* 0.0181 *shi #1*:*Rab11 #2* 0.0428 *shi #2*:*Rab5 #2* 0.0263 *Rab5 #1*:*Rab5 #2* 0.0009 *Rab5 #1*:*Rab11 #2* 0.0020 all others, ns
Figure 3C	6–10	2–3	see 3-S1A	see ***Figure 3—figure supplement 1A***
Figure 3E	4–5	3	Unpaired t-test	Apical region: Pre:Post < 0.0001
Figure 3P	3–4	2	Unpaired t-test	WT:*shi RNAi* < 0.0001
Figure 4B	3–4	2	Unpaired t-test	Pre:Post < 0.0001
Figure 4F	13–14	2	One-way ANOVA with Tukey's multiple comparisons test	ANOVA:<0.0001 WT:$ogre^{DN}$ < 0.0001 WT:*Df* < 0.0001 WT:*ogre RNAi* 0.0007
Figure 4H	27–37	3	One-way ANOVA with Tukey's multiple comparisons test (mean death at 10 days in each group)	ANOVA:<0.0001 WTsalt:shi^{DN}reg ns, 0.7173 WTsalt:shi^{DN}salt < 0.0001 shi^{DN}salt:shi^{DN}reg < 0.0001 ANOVA:<0.0001 WTsalt:$ogre^{DN}$reg < 0.0001 WTsalt:$ogre^{DN}$salt < 0.0001 $ogre^{DN}$salt:$ogre^{DN}$reg < 0.0001
Figure 1—figure supplement 1H	12–20	2	Unpaired t-test	WT:*fzr RNAi* < 0.0001 WT:N^{DN} ns, 0.1786
Figure 2—figure supplement 1A	8–11	2	One-way ANOVA with Tukey's multiple comparisons test	ANOVA:<0.0001 *Sing RNAi*:all others < 0.0001 All others: ns
Figure 2—figure supplement 1B	6–8	2	One-way ANOVA	ANOVA: ns, 0.3692
Figure 2—figure supplement 1C	11–23	2	One-way ANOVA with Tukey's multiple comparisons test	ANOVA: 0.0044 *shi RNAi #1*:*Rab11 RNAi #1* 0.0244 *Rab5 RNAi #2*:*Rab11 RNAi #1* 0.0193 All others: ns
Figure 2—figure supplement 1F	10–11	2	Unpaired t-test	ns, 0.0782
Figure 3—figure supplement 1A	6–10	2	One-way ANOVA with Tukey's multiple comparisons test	ANOVA:<0.0001 Pre:Post < 0.0001 Pre:*shi RNAi* ns, 0.7882 Post:*shi RNAi* < 0.0001
Figure 3—figure supplement 1B''	10	2	Unpaired t-test	Apical basal difference (see 1-S3A) Pre:Post 0.0007
Figure 3—figure supplement 1G	3–4	2	Unpaired t-test	ns, 0.2203
Figure 3—figure supplement 1G'	3–4	2	Unpaired t-test	ns, 0.4754

Table 6 continued on next page

Table 6 continued

Panel	N (animals) per group	Bio. reps	Statistical test	P-value
Figure 3—figure supplement 1G''	3–4	2	Multiple unpaired t-tests	Septate: WT:*shi RNAi* ns, 0.1547 Gap: WT:*shi RNAi* < 0.0001
Figure 4—figure supplement 1A	3–4	2	One-way ANOVA	ns, 0.8973
Figure 4—figure supplement 1A'	3–4	2	One-way ANOVA	ns, 0.3994
Figure 4—figure supplement 1A''	3–4	2	Multiple unpaired t-tests	Septate: all ns Gap: Pre:Post 0.0004 Gap: all others, ns
Figure 4—figure supplement 1E''	11	2	Unpaired t-test	WT:shi^{DN} < 0.0001

Line profiles

For line profile data collection, fixed and mounted hindguts were imaged on a Zeiss Apotome on the 40Xoil objective. Once moved into ImageJ, the images were rotated with no interpolation so that the central canal was perpendicular to the bottom of the image. From the midline of the central canal, a straight line (width of 300) was drawn out to one edge of the papillae. One papilla was measured per animal. Papillae were measured at the widest width. Next, the Analyze > Plot Profile data was collected from this representative 300 width line and moved into Excel. In Excel, the data was first was normalized to the maximum length of the papillae and the maximum GFP intensity per animal. Each data point is a % of the total length of the papillae and a % of the maximum GFP intensity. Next, the X values were rounded to its nearest 1% value. Next, all the Y-values were averaged per X value bins (average % GFP intensity per rounded % distance value). % GFP intensity values were plotted from 1–100% total distance of papilla.

Statistical analysis

Statistical analysis was performed in GraphPad Prism 8. Detailed statistical tests and methods are reported in ***Table 6***.

Genotype and experiment-specific method notes

Some additional methodological details, including animal genotype, applied to only a specific figure panel. Please see ***Table 6*** for this information.

Acknowledgements

We thank members of the Fox laboratory and Drs. Dong Yan and Tony Harris for valuable feedback. Ying Hao (Duke Eye Center) provided assistance with electron microscopy. The Duke Light Microscopy Core Facility supplied training and microscopes that were used for live and fixed fluoresecence microscopy. Jamie Roebuck (Duke University) generated the transgenic *UAS-Gapdh2-GFP*^{PA} flies.

Additional information

Funding

Funder	Grant reference number	Author
National Institutes of Health	GM118447	Donald T Fox
National Institutes of Health	HL140811	Nora G Peterson

The funders had no role in study design, data collection and interpretation, or the decision to submit the work for publication.

Author contributions

Nora G Peterson, Juliet S King, Conceptualization, Resources, Data curation, Software, Formal analysis, Supervision, Funding acquisition, Validation, Investigation, Visualization, Methodology, Writing - original draft, Project administration, Writing - review and editing; Benjamin M Stormo, Conceptualization, Resources, Data curation, Formal analysis, Validation, Investigation, Visualization, Methodology; Kevin P Schoenfelder, Conceptualization, Resources, Data curation, Software, Formal analysis, Validation, Investigation, Visualization, Methodology; Rayson RS Lee, Resources, Data curation, Formal analysis, Validation, Investigation, Visualization; Donald T Fox, Conceptualization, Supervision, Funding acquisition, Visualization, Writing - original draft, Project administration, Writing - review and editing

Author ORCIDs

Nora G Peterson https://orcid.org/0000-0002-7734-1861
Benjamin M Stormo http://orcid.org/0000-0002-6861-8451
Donald T Fox https://orcid.org/0000-0002-0436-179X

Decision letter and Author response

Decision letter https://doi.org/10.7554/eLife.58107.sa1
Author response https://doi.org/10.7554/eLife.58107.sa2

Additional files

Supplementary files

- Transparent reporting form

Data availability

All data generated or analyzed during this study are included in the manuscript and supporting files.

The following previously published dataset was used:

Author(s)	Year	Dataset title	Dataset URL	Database and Identifier
Leader DP, Krause SA, Pandit A, Davies SA, Dow JAT	2018	FlyAtlas2	http://flyatlas.gla.ac.uk/FlyAtlas2/index.html	FlyAtlas, 10.1093/nar/gkx976

References

Asare A, Levorse J, Fuchs E. 2017. Coupling organelle inheritance with mitosis to balance growth and differentiation. *Science* **355**:eaah4701. DOI: https://doi.org/10.1126/science.aah4701, PMID: 28154022

Audsley N, Weaver RJ. 2009. Neuropeptides associated with the regulation of feeding in insects. *General and Comparative Endocrinology* **162**:93–104. DOI: https://doi.org/10.1016/j.ygcen.2008.08.003, PMID: 18775723

Augustin H, McGourty K, Allen MJ, Madem SK, Adcott J, Kerr F, Wong CT, Vincent A, Godenschwege T, Boucrot E, Partridge L. 2017. Reduced insulin signaling maintains electrical transmission in a neural circuit in aging flies. *PLOS Biology* **15**:e2001655. DOI: https://doi.org/10.1371/journal.pbio.2001655, PMID: 28902870

Avner ED, Sweeney WE, Nelson WJ. 1992. Abnormal sodium pump distribution during renal tubulogenesis in congenital murine polycystic kidney disease. *PNAS* **89**:7447–7451. DOI: https://doi.org/10.1073/pnas.89.16.7447, PMID: 1323837

Bauer R, Löer B, Ostrowski K, Martini J, Weimbs A, Lechner H, Hoch M. 2005. Intercellular communication: the *Drosophila* innexin multiprotein family of gap junction proteins. *Chemistry & Biology* **12**:515–526. DOI: https://doi.org/10.1016/j.chembiol.2005.02.013, PMID: 15911372

Berridge MJ, Gupta BL. 1967. Fine-Structural changes in relation to ion and water transport in rectal papillae of blowfly Calliphora. *Journal of Cell Science* **2**:89. PMID: 6031010

Bischoff M, Gradilla AC, Seijo I, Andrés G, Rodríguez-Navas C, González-Méndez L, Guerrero I. 2013. Cytonemes are required for the establishment of a normal hedgehog morphogen gradient in *Drosophila* epithelia. *Nature Cell Biology* **15**:1269–1281. DOI: https://doi.org/10.1038/ncb2856, PMID: 24121526

Bretscher HS, Fox DT. 2016. Proliferation of Double-Strand Break-Resistant polyploid cells requires *Drosophila* FANCD2. *Developmental Cell* **37**:444–457. DOI: https://doi.org/10.1016/j.devcel.2016.05.004, PMID: 27270041

Brunetti TM, Fremin BJ, Cripps RM. 2015. Identification of singles bar as a direct transcriptional target of *Drosophila* myocyte enhancer factor-2 and a regulator of adult myoblast fusion. *Developmental Biology* **401**:299–309. DOI: https://doi.org/10.1016/j.ydbio.2015.02.026, PMID: 25797154

Cieniewicz AM, Woodruff RI. 2010. Passage through vertebrate gap junctions of 17/18kDa molecules is primarily dependent upon molecular configuration. *Tissue and Cell* **42**:47–52. DOI: https://doi.org/10.1016/j.tice.2009.07.003, PMID: 19726067

Cohen E, Sawyer JK, Peterson NG, Dow JAT, Fox DT. 2020. Physiology, development, and disease modeling in the *Drosophila* Excretory System. *Genetics* **214**:235–264. DOI: https://doi.org/10.1534/genetics.119.302289, PMID: 32029579

Conlon I, Raff M. 1999. Size control in animal development. *Cell* **96**:235–244. DOI: https://doi.org/10.1016/S0092-8674(00)80563-2, PMID: 9988218

Curtin KD, Zhang Z, Wyman RJ. 1999. *Drosophila* has several genes for gap junction proteins. *Gene* **232**:191–201. DOI: https://doi.org/10.1016/S0378-1119(99)00123-7, PMID: 10352230

Damke H, Baba T, Warnock DE, Schmid SL. 1994. Induction of mutant dynamin specifically blocks endocytic coated vesicle formation. *Journal of Cell Biology* **127**:915–934. DOI: https://doi.org/10.1083/jcb.127.4.915

Datta SR, Vasconcelos ML, Ruta V, Luo S, Wong A, Demir E, Flores J, Balonze K, Dickson BJ, Axel R. 2008. The *Drosophila* pheromone cVA activates a sexually dimorphic neural circuit. *Nature* **452**:473–477. DOI: https://doi.org/10.1038/nature06808, PMID: 18305480

Deng S, Azevedo M, Baylies M. 2017. Acting on identity: myoblast fusion and the formation of the syncytial muscle fiber. *Seminars in Cell & Developmental Biology* **72**:45–55. DOI: https://doi.org/10.1016/j.semcdb.2017.10.033, PMID: 29101004

Doane JA, Purdy K, Pasternak S. 2015. Generalized multinucleate cell angiohistiocytoma. *Journal of Cutaneous Medicine and Surgery* **19**:323–325. DOI: https://doi.org/10.2310/7750.2014.14129, PMID: 25775651

Dunk CE, Gellhaus A, Drewlo S, Baczyk D, Pötgens AJ, Winterhager E, Kingdom JC, Lye SJ. 2012. The molecular role of connexin 43 in human trophoblast cell fusion. *Biology of Reproduction* **86**:115. DOI: https://doi.org/10.1095/biolreprod.111.096925, PMID: 22238282

Estrada B, Maeland AD, Gisselbrecht SS, Bloor JW, Brown NH, Michelson AM. 2007. The MARVEL domain protein, singles bar, is required for progression past the pre-fusion complex stage of myoblast fusion. *Developmental Biology* **307**:328–339. DOI: https://doi.org/10.1016/j.ydbio.2007.04.045, PMID: 17537424

Eugenin EA, Gaskill PJ, Berman JW. 2009. Tunneling nanotubes (TNT) are induced by HIV-infection of macrophages: a potential mechanism for intercellular HIV trafficking. *Cellular Immunology* **254**:142–148. DOI: https://doi.org/10.1016/j.cellimm.2008.08.005, PMID: 18835599

Fabrowski P, Necakov AS, Mumbauer S, Loeser E, Reversi A, Streichan S, Briggs JA, De Renzis S. 2013. Tubular endocytosis drives remodelling of the apical surface during epithelial morphogenesis in *Drosophila*. *Nature Communications* **4**:2244. DOI: https://doi.org/10.1038/ncomms3244, PMID: 23921440

Faust JJ, Balabiyev A, Heddleston JM, Podolnikova NP, Baluch DP, Chew TL, Ugarova TP. 2019. An actin-based protrusion originating from a podosome-enriched region initiates macrophage fusion. *Molecular Biology of the Cell* **30**:2254–2267. DOI: https://doi.org/10.1091/mbc.E19-01-0009, PMID: 31242090

Filosa JN, Berry CT, Ruthel G, Beverley SM, Warren WC, Tomlinson C, Myler PJ, Dudkin EA, Povelones ML, Povelones M. 2019. Dramatic changes in gene expression in different forms of Crithidia fasciculata reveal potential mechanisms for insect-specific adhesion in kinetoplastid parasites. *PLOS Neglected Tropical Diseases* **13**:e0007570. DOI: https://doi.org/10.1371/journal.pntd.0007570, PMID: 31356610

Firth JA, Farr A, Bauman K. 1980. The role of gap junctions in trophoblastic cell fusion in the guinea-pig placenta. *Cell and Tissue Research* **205**:311–318. DOI: https://doi.org/10.1007/BF00234689, PMID: 7357576

Fox DT, Gall JG, Spradling AC. 2010. Error-prone polyploid mitosis during normal *Drosophila* development. *Genes & Development* **24**:2294–2302. DOI: https://doi.org/10.1101/gad.1952710, PMID: 20952538

Garayoa M, Villaro AC, Lezaun MJ, Sesma P. 1999. Light and electron microscopic study of the hindgut of the ant (Formica nigricans, hymenoptera): II. structure of the rectum. *Journal of Morphology* **242**:205–228. DOI: https://doi.org/10.1002/(SICI)1097-4687(199912)242:3<205::AID-JMOR2>3.0.CO;2-#, PMID: 10580261

Gerbaud P, Pidoux G. 2015. Review: an overview of molecular events occurring in human trophoblast fusion. *Placenta* **36**:S35–S42. DOI: https://doi.org/10.1016/j.placenta.2014.12.015, PMID: 25564303

Gilleron J, Carette D, Fiorini C, Dompierre J, Macia E, Denizot JP, Segretain D, Pointis G. 2011. The large GTPase dynamin2: a new player in connexin 43 gap junction endocytosis, recycling and degradation. *The*

International Journal of Biochemistry & Cell Biology **43**:1208–1217. DOI: https://doi.org/10.1016/j.biocel.2011.04.014, PMID: 21554976

Gillooly DJ, Morrow IC, Lindsay M, Gould R, Bryant NJ, Gaullier JM, Parton RG, Stenmark H. 2000. Localization of phosphatidylinositol 3-phosphate in yeast and mammalian cells. *The EMBO Journal* **19**:4577–4588. DOI: https://doi.org/10.1093/emboj/19.17.4577, PMID: 10970851

Greenbaum MP, Iwamori T, Buchold GM, Matzuk MM. 2011. Germ cell intercellular bridges. *Cold Spring Harbor Perspectives in Biology* **3**:a005850. DOI: https://doi.org/10.1101/cshperspect.a005850, PMID: 21669984

Gu JB, Dong YQ, Peng HJ, Chen XG. 2010. A recombinant AeDNA containing the insect-specific toxin, BmK IT1, displayed an increasing pathogenicity on aedes albopictus. *The American Journal of Tropical Medicine and Hygiene* **83**:614–623. DOI: https://doi.org/10.4269/ajtmh.2010.10-0074, PMID: 20810829

Gupta BL, Berridge MJ. 1966. Fine structural organization of the rectum in the blowfly, Calliphora erythrocephala (Meig.) with special reference to connective tissue, tracheae and neurosecretory innervation in the rectal papillae. *Journal of Morphology* **120**:23–81. DOI: https://doi.org/10.1002/jmor.1051200104, PMID: 5969374

Habas mantel L, Mantel LH. 1968. The foregut of *Gecarcinus lateralis* as an organ of salt and water balance. *American Zoologist* **8**:433–442. DOI: https://doi.org/10.1093/icb/8.3.433

Hampel S, Chung P, McKellar CE, Hall D, Looger LL, Simpson JH. 2011. *Drosophila* brainbow: a recombinase-based fluorescence labeling technique to subdivide neural expression patterns. *Nature Methods* **8**:253–259. DOI: https://doi.org/10.1038/nmeth.1566, PMID: 21297621

Hasegawa K, Suetsugu A, Nakamura M, Matsumoto T, Aoki H, Kunisada T, Shimizu M, Saji S, Moriwaki H, Hoffman RM. 2017. Imaging the role of multinucleate pancreatic Cancer cells and Cancer-Associated fibroblasts in peritoneal metastasis in mouse models. *Anticancer Research* **37**:3435–3440. DOI: https://doi.org/10.21873/anticanres.11711, PMID: 28668832

Hinshaw JE, Schmid SL. 1995. Dynamin self-assembles into rings suggesting a mechanism for coated vesicle budding. *Nature* **374**:190–192. DOI: https://doi.org/10.1038/374190a0, PMID: 7877694

Holcroft CE, Jackson WD, Lin WH, Bassiri K, Baines RA, Phelan P. 2013. Innexins ogre and Inx2 are required in glial cells for normal postembryonic development of the *Drosophila* central nervous system. *Journal of Cell Science* **126**:3823–3834. DOI: https://doi.org/10.1242/jcs.117994, PMID: 23813964

Hopkins CR. 1967. The fine-structural changes observed in the rectal papillae of the mosquito aedes aegypti, L. and their relation to the epithelial transport of water and inorganic ions. *Journal of the Royal Microscopical Society* **86**:235–252. DOI: https://doi.org/10.1111/j.1365-2818.1967.tb00585.x

Ikebe H, Takamatsu T, Itoi M, Fujita S. 1986. Age-dependent changes in nuclear DNA content and cell size of presumably normal human corneal endothelium. *Experimental Eye Research* **43**:251–258. DOI: https://doi.org/10.1016/S0014-4835(86)80093-8, PMID: 3758224

Johnson RI, Sedgwick A, D'Souza-Schorey C, Cagan RL. 2011. Role for a Cindr-Arf6 Axis in patterning emerging epithelia. *Molecular Biology of the Cell* **22**:4513–4526. DOI: https://doi.org/10.1091/mbc.e11-04-0305, PMID: 21976699

Kim JH, Jin P, Duan R, Chen EH. 2015. Mechanisms of myoblast fusion during muscle development. *Current Opinion in Genetics & Development* **32**:162–170. DOI: https://doi.org/10.1016/j.gde.2015.03.006, PMID: 25989064

Lajevardi A, Paluzzi JV. 2020. Receptor characterization and functional activity of pyrokinins on the hindgut in the adult mosquito, *Aedes aegypti*. *Frontiers in Physiology* **11**:490. DOI: https://doi.org/10.3389/fphys.2020.00490, PMID: 32528310

Laprise P, Lau KM, Harris KP, Silva-Gagliardi NF, Paul SM, Beronja S, Beitel GJ, McGlade CJ, Tepass U. 2009. Yurt, coracle, neurexin IV and the na(+),K(+)-ATPase form a novel group of epithelial polarity proteins. *Nature* **459**:1141–1145. DOI: https://doi.org/10.1038/nature08067, PMID: 19553998

Leader DP, Krause SA, Pandit A, Davies SA, Dow JAT. 2018. FlyAtlas 2: a new version of the *Drosophila melanogaster* expression atlas with RNA-Seq, miRNA-Seq and sex-specific data. *Nucleic Acids Research* **46**:D809–D815. DOI: https://doi.org/10.1093/nar/gkx976, PMID: 29069479

Lehmann C, Lechner H, Löer B, Knieps M, Herrmann S, Famulok M, Bauer R, Hoch M. 2006. Heteromerization of innexin gap junction proteins regulates epithelial tissue organization in *Drosophila*. *Molecular Biology of the Cell* **17**:1676–1685. DOI: https://doi.org/10.1091/mbc.e05-11-1059, PMID: 16436513

Linneweber GA, Winking M, Fischbach KF. 2015. The cell adhesion molecules roughest, Hibris, kin of irre and sticks and stones are required for long range spacing of the *Drosophila* wing disc sensory sensilla. *PLOS ONE* **10**:e0128490. DOI: https://doi.org/10.1371/journal.pone.0128490, PMID: 26053791

Losick VP, Fox DT, Spradling AC. 2013. Polyploidization and cell fusion contribute to wound healing in the *adult Drosophila* epithelium. *Current Biology* **23**:2224–2232. DOI: https://doi.org/10.1016/j.cub.2013.09.029, PMID: 24184101

Lowne BT. 1869. I.-On the redal papillae of the fly. *The Monthly Microscopical Journal* **2**:1–4. DOI: https://doi.org/10.1111/j.1365-2818.1869.tb05619.x

Lůcas WJ, Wolf S. 1993. Plasmodesmata: the intercellular organelles of green plants. *Trends in Cell Biology* **3**:308–315. DOI: https://doi.org/10.1016/0962-8924(93)90013-Q, PMID: 14731848

Mahowald AP. 1971. The formation of ring canals by cell furrows in *Drosophila*. *Zeitschrift für Zellforschung Und Mikroskopische Anatomie* **118**:162–167. DOI: https://doi.org/10.1007/BF00341561

Mancini I, Righi A, Gambarotti M, Picci P, Dei Tos AP, Billings SD, Simi L, Franchi A. 2017. Phenotypic and molecular differences between giant-cell tumour of soft tissue and its bone counterpart. *Histopathology* **71**:453–460. DOI: https://doi.org/10.1111/his.13249, PMID: 28477388

Martin SG. 2016. Role and organization of the actin cytoskeleton during cell-cell fusion. *Seminars in Cell & Developmental Biology* **60**:121–126. DOI: https://doi.org/10.1016/j.semcdb.2016.07.025, PMID: 27476112

Maunsbach AB. 1966. Observations on the segmentation of the proximal tubule in the rat kidney comparison of results from phase contrast, fluorescence and electron microscopy. *Journal of Ultrastructure Research* **16**:239–258. DOI: https://doi.org/10.1016/s0022-5320(66)80060-6, PMID: 5333381

McLean PF, Cooley L. 2013. Protein equilibration through somatic ring canals in *Drosophila*. *Science* **340**:1445–1447. DOI: https://doi.org/10.1126/science.1234887, PMID: 23704373

Molitoris BA, Dahl R, Geerdes A. 1992. Cytoskeleton disruption and apical redistribution of proximal tubule na (+)-K(+)-ATPase during ischemia. *American Journal of Physiology-Renal Physiology* **263**:F488–F495. DOI: https://doi.org/10.1152/ajprenal.1992.263.3.F488

Mueller RL. 2015. Genome biology and the evolution of Cell-Size diversity. *Cold Spring Harbor Perspectives in Biology* **7**:a019125. DOI: https://doi.org/10.1101/cshperspect.a019125, PMID: 26254312

Palm NB. 1949. *The Rectal Papillae in Insects*. Lunds universitets a˚rsskrift W.K. Gleerup.

Patrick ML, Aimanova K, Sanders HR, Gill SS. 2006. P-type na+/K+-ATPase and V-type H+-ATPase expression patterns in the osmoregulatory organs of larval and adult mosquito aedes aegypti. *Journal of Experimental Biology* **209**:4638–4651. DOI: https://doi.org/10.1242/jeb.02551, PMID: 17114398

Pease DC. 1955. Electron microscopy of the tubular cells of the kidney cortex. *The Anatomical Record* **121**:723–743. DOI: https://doi.org/10.1002/ar.1091210403, PMID: 14388261

Pease DC. 1956. Infolded basal plasma membranes found in Epithelia noted for their water transport. *The Journal of Biophysical and Biochemical Cytology* **2**:203–208. DOI: https://doi.org/10.1083/jcb.2.4.203, PMID: 13357543

Peifer M, Orsulic S, Sweeton D, Wieschaus E. 1993. A role for the *Drosophila* segment polarity gene Armadillo in cell adhesion and cytoskeletal integrity during oogenesis. *Development* **118**:1191–1207. PMID: 8269848

Pereira M, Petretto E, Gordon S, Bassett JHD, Williams GR, Behmoaras J. 2018. Common signalling pathways in macrophage and osteoclast multinucleation. *Journal of Cell Science* **131**:jcs216267. DOI: https://doi.org/10.1242/jcs.216267, PMID: 29871956

Petrany MJ, Millay DP. 2019. Cell fusion: merging membranes and making muscle. *Trends in Cell Biology* **29**:964–973. DOI: https://doi.org/10.1016/j.tcb.2019.09.002, PMID: 31648852

Phelan P, Stebbings LA, Baines RA, Bacon JP, Davies JA, Ford C. 1998. *Drosophila* Shaking-B protein forms gap junctions in paired *Xenopus* oocytes. *Nature* **391**:181–184. DOI: https://doi.org/10.1038/34426, PMID: 9428764

Rebay I, Fehon RG, Artavanis-Tsakonas S. 1993. Specific truncations of *Drosophila* notch define dominant activated and dominant negative forms of the receptor. *Cell* **74**:319–329. DOI: https://doi.org/10.1016/0092-8674(93)90423-N, PMID: 8343959

Richard M, Bauer R, Tavosanis G, Hoch M. 2017. The gap junction protein Innexin3 is required for eye disc growth in *Drosophila*. *Developmental Biology* **425**:191–207. DOI: https://doi.org/10.1016/j.ydbio.2017.04.001, PMID: 28390801

Richardson BE, Beckett K, Nowak SJ, Baylies MK. 2007. SCAR/WAVE and Arp2/3 are crucial for cytoskeletal remodeling at the site of myoblast fusion. *Development* **134**:4357–4367. DOI: https://doi.org/10.1242/dev.010678, PMID: 18003739

Rocco DA, Kim DH, Paluzzi JV. 2017. Immunohistochemical mapping and transcript expression of the GPA2/GPB5 receptor in tissues of the adult mosquito, aedes aegypti. *Cell and Tissue Research* **369**:313–330. DOI: https://doi.org/10.1007/s00441-017-2610-3, PMID: 28401307

Rueden CT, Schindelin J, Hiner MC, DeZonia BE, Walter AE, Arena ET, Eliceiri KW. 2017. ImageJ2: imagej for the next generation of scientific image data. *BMC Bioinformatics* **18**:1934-z. DOI: https://doi.org/10.1186/s12859-017-1934-z

Rustom A, Saffrich R, Markovic I, Walther P, Gerdes HH. 2004. Nanotubular highways for intercellular organelle transport. *Science* **303**:1007–1010. DOI: https://doi.org/10.1126/science.1093133, PMID: 14963329

Sawamiphak S, Kontarakis Z, Filosa A, Reischauer S, Stainier DYR. 2017. Transient cardiomyocyte fusion regulates cardiac development in zebrafish. *Nature Communications* **8**:1525. DOI: https://doi.org/10.1038/s41467-017-01555-8, PMID: 29142194

Schilling AF, Filke S, Lange T, Gebauer M, Brink S, Baranowsky A, Zustin J, Amling M. 2008. Gap junctional communication in human osteoclasts *in vitro* and *in vivo*. *Journal of Cellular and Molecular Medicine* **12**:2497–2504. DOI: https://doi.org/10.1111/j.1582-4934.2008.00275.x, PMID: 18266960

Schindelin J, Arganda-Carreras I, Frise E, Kaynig V, Longair M, Pietzsch T, Preibisch S, Rueden C, Saalfeld S, Schmid B, Tinevez J-Y, White DJ, Hartenstein V, Eliceiri K, Tomancak P, Cardona A. 2012. Fiji: an open-source platform for biological-image analysis. *Nature Methods* **9**:676–682. DOI: https://doi.org/10.1038/nmeth.2019

Schoenfelder KP, Montague RA, Paramore SV, Lennox AL, Mahowald AP, Fox DT. 2014. Indispensable pre-mitotic endocycles promote aneuploidy in the *Drosophila* rectum. *Development* **141**:3551–3560. DOI: https://doi.org/10.1242/dev.109850, PMID: 25142462

Schoenfelder KP, Fox DT. 2015. The expanding implications of polyploidy. *Journal of Cell Biology* **209**:485–491. DOI: https://doi.org/10.1083/jcb.201502016, PMID: 26008741

Sens KL, Zhang S, Jin P, Duan R, Zhang G, Luo F, Parachini L, Chen EH. 2010. An invasive podosome-like structure promotes fusion pore formation during myoblast fusion. *Journal of Cell Biology* **191**:1013–1027. DOI: https://doi.org/10.1083/jcb.201006006, PMID: 21098115

Singer JB, Harbecke R, Kusch T, Reuter R, Lengyel JA. 1996. *Drosophila* brachyenteron regulates gene activity and morphogenesis in the gut. *Development* **122**:3707–3718. PMID: 9012492

Sjöstrand FS, Rhodin J. 1953. The ultrastructure of the proximal convoluted tubules of the mouse kidney as revealed by high resolution electron microscopy. *Experimental Cell Research* **4**:426–456. DOI: https://doi.org/10.1016/0014-4827(53)90170-0

Smurova K, Podbilewicz B. 2016. RAB-5- and DYNAMIN-1-Mediated endocytosis of EFF-1 fusogen controls Cell-Cell fusion. *Cell Reports* **14**:1517–1527. DOI: https://doi.org/10.1016/j.celrep.2016.01.027, PMID: 26854231

Spéder P, Brand AH. 2014. Gap junction proteins in the blood-brain barrier control nutrient-dependent reactivation of *Drosophila* neural stem cells. *Developmental Cell* **30**:309–321. DOI: https://doi.org/10.1016/j.devcel.2014.05.021, PMID: 25065772

Stormo BM, Fox DT. 2016. Distinct responses to reduplicated chromosomes require distinct Mad2 responses. *eLife* **5**:e15204. DOI: https://doi.org/10.7554/eLife.15204, PMID: 27159240

Stormo BM, Fox DT. 2019. Interphase cohesin regulation ensures mitotic fidelity after genome reduplication. *Molecular Biology of the Cell* **30**:219–227. DOI: https://doi.org/10.1091/mbc.E17-10-0582, PMID: 30462577

Van de Peer Y, Mizrachi E, Marchal K. 2017. The evolutionary significance of polyploidy. *Nature Reviews Genetics* **18**:411–424. DOI: https://doi.org/10.1038/nrg.2017.26, PMID: 28502977

Waldo GS, Standish BM, Berendzen J, Terwilliger TC. 1999. Rapid protein-folding assay using green fluorescent protein. *Nature Biotechnology* **17**:691–695. DOI: https://doi.org/10.1038/10904, PMID: 10404163

Wessing A, Eichelberg D. 1973. [Electron microscopic studies on structure and function of the rectal papillae in *Drosophila melanogaster*]. *Zeitschrift Fur Zellforschung Und Mikroskopische Anatomie* **136**:415–432. PMID: 4630996

Wigglesworth VB. 1932. On the function of the so-called 'rectal glands' of insects. *Quarterly Journal of Microscopical Science* **75**:131–150.

Wucherpfennig T, Wilsch-Bräuninger M, González-Gaitán M. 2003. Role of *Drosophila* Rab5 during endosomal trafficking at the synapse and evoked neurotransmitter release. *Journal of Cell Biology* **161**:609–624. DOI: https://doi.org/10.1083/jcb.200211087, PMID: 12743108

Xing G, Li M, Sun Y, Rui M, Zhuang Y, Lv H, Han J, Jia Z, Xie W. 2018. Neurexin-Neuroligin 1 regulates synaptic morphology and functions via the WAVE regulatory complex in *Drosophila* neuromuscular junction. *eLife* **7**:e30457. DOI: https://doi.org/10.7554/eLife.30457, PMID: 29537369